Polymer Process Design for Clinical Validation of Early Medical Technologies: Applications for a Micro-fluidic Cartridge

A thesis submitted by

Kenneth P. Vandevoordt

In partial fulfillment of requirements for the degree of

Master of Science

in

Mechanical Engineering

TUFTS UNIVERSITY

February 2015

ADVISORS:

Kumaran Kolandaivelu, MD, PhD, Brigham and Women's Hospital, Massachusetts Institute of Technology Clinical Research Center

Jason Rife, PhD, Department of Mechanical Engineering, Tufts University

COMMITTEE MEMBER:

Anil Saigal, PhD, Department of Mechanical Engineering, Tufts University

ABSTRACT

Prototype medical devices developed to prove laboratory science are manufactured at small quantities for bench-top testing; however, in order to provide high quality clinical data for validation, production must be scaled up to make hundreds of devices for clinical trials. One example of a device undergoing this transition to clinical trials is a disposable micro-fluidic cartridge designed to study blood clotting at Massachusetts Institute of Technology's Clinical Research Center. This thesis aims to down-select from a variety of polymer processing techniques to determine the appropriate method to create these micro-fluidic cartridges for clinical trials. Additionally, this thesis develops a modeling technique used to predict the robustness of the selected manufacturing process. The modeling technique and manufacturing process are then used to redesign and build cartridge parts for clinical trials.

ACKNOWLEDGEMENTS

I would like to express the deepest appreciation to my advisor, Kumaran Kolandaivelu, for his guidance and support. I also wish to thank the other members of my examining committee, Professors Jason Rife and Anil Saigal.

I wish to thank the Charles Stark Draper Laboratory for supporting this research and my graduate education. In particular, thank you Vijay Kolachalama and Cathy McEleney from Draper Laboratory for their patient instruction and insightful advice.

I also thank my friends and family who have supported me during this research. Thank you to my parents for their support throughout my entire academic career. A special thank you to my wife, Shannon, for her continuing encouragement.

Table of Contents

List of Figures

List of Tables

1. Introduction

1.1. Motivation

Many medical devices and their underlying science are developed in a laboratory setting where hardware is needed at the prototype design level in small quantities. Once a device has proven value at the prototype (bench-top) stage it typically progresses to clinical trials (bedside) [1]. Research findings that are transitioned from the researcher's bench to the patient's bedside and community are defined as translational research [2, 3].

One factor making translational research difficult is that developers at this stage often do not have significant resources due to the unproven device effectiveness on a broad population. Additionally, larger quantities of hardware are typically needed to develop medical devices for clinical trials; this is especially true for products containing disposable, single-use hardware. Scaling up disposable hardware production must meet clinical trial quantities and consistency. Yet, such production can be expensive and time-consuming using typical prototyping methods such as 3-D printing or computer numerically controlled (CNC) machining, or alternatively mass-scale manufacturing where fixed overhead costs may be prohibitive. The

ability to consistently manufacture parts is critical for clinical trials so that result variations from these trials can be attributed to factors that are independent of the quality of parts used in testing.

In order to reduce a device's time to market and the cost associated with reaching clinical trials, specific manufacturing methods and materials must be selected based on these principles. By performing a methodological study of techniques and materials used to produce clinical trial hardware of disposal medical devices, we hope to provide an efficient path forward for enabling and accelerating translational research.

1.2. Case Study: Micro-fluidic Cartridge

An example of translational research that forms the foundation for this thesis is a disposable micro-fluidic cartridge designed and built to study blood clotting at the Institute for Medical Engineering and Sciences Clinical Research Center (CRC) at the Massachusetts Institute of Technology (MIT). Blood clotting, or thrombosis, is a critical issue that affects millions of people each year [4]. If it occurs excessively, it can lead to myocardial infarction (heart attack) or stroke, two of the leading causes of mortality in the United States [5, 6]. If insufficient treatment is received, it can cause catastrophic hemorrhage – resulting in over 30% of fatalities in trauma and combat victims [7, 8]. Clinically, thrombosis is managed through the use of medicines that increase or decrease an individual's ability to form clot [9, 10, 11]. Yet, it

remains unclear how these various drugs should best be administered to a particular patient [12, 13, 14, 15, 16, 17, 18]. Current research at CRC has developed a platform by which an individual's 'clotting profile' can be monitored in high resolution and is at a critical juncture in transitioning from the bench-top to clinical applications.

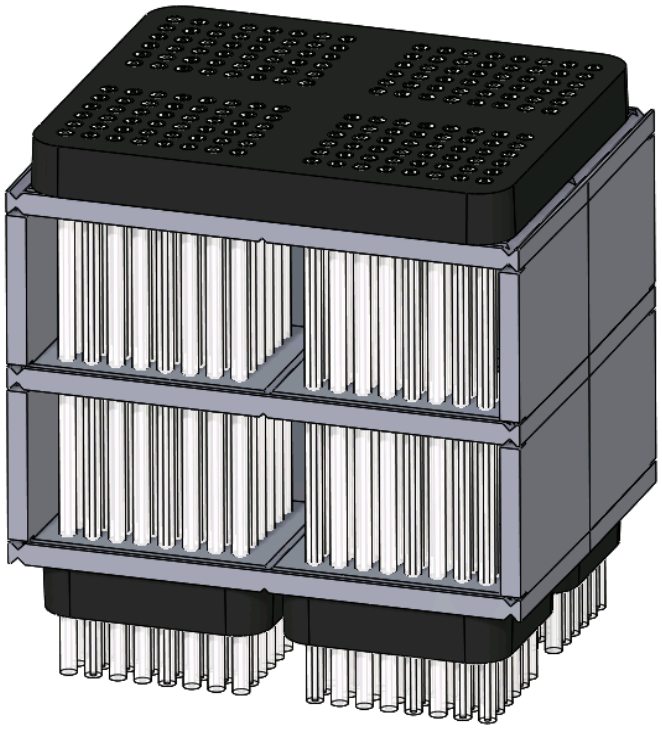

Figure 1 - Micro-Fluidic Cartridge Assembly

The platform developed by at CRC consists of an assay detection fixture containing optical transducers, signal analysis equipment, and a feed plenum. The plenum supplies blood to a single-use micro-fluidic cartridge, shown in Figure 1. As designed, the cartridge frame uses I-beam structures, called *lateral walls*, that separates plates, called *array plates,* to hold a series of

parallel capillary tubes in close alignment, while providing overall structural rigidity. The frame and tubes are further integrated into a series of silicone gaskets. An exploded view of the cartridge can be found in Figure 2. When the cartridge is fully assembled, it is placed into the fixture and supplied with blood. Clot forms in the tubes and is then quantified using an optical sensor; each signal is then integrated into an overall pattern that represents an individual's propensity to clot or bleed.

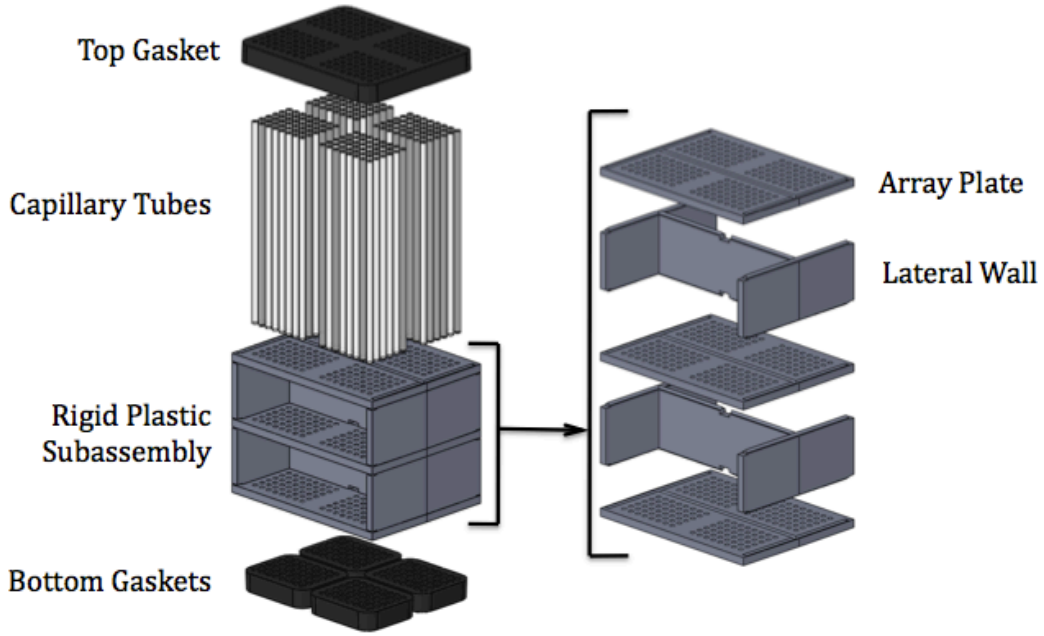

Figure 2 - Micro-Fluidic Cartridge, Exploded View

Prototype cartridges for bench-top use have been built using commercial-off-the-shelf (COTS) capillary tubes, custom molded gaskets, and 3-D printed rigid plastic subassembly parts for research use in the laboratory. The disposable cartridge units currently cost more than $150 per unit and are constructed on the scale of tens of assemblies. Going forward, manufacturing

quantities will need to increase to three to five hundred devices for early clinical validation testing and costs must be reduced to less than $5 material costs per unit. Along with the quantity and cost requirements, it is also necessary to maintain overall shape and number of tubes per cartridge to enable proper mating between the cartridge and fixture, as well as optical read out.

Broadly, this thesis also looks to take advantage of a growing collaboration between the CRC and the Charles Stark Draper Laboratory (Draper) that seeks to accelerate the R&D cycle of early stage medical technologies. Manufacturing of the cartridges will occur at Draper Laboratory while device testing will be accomplished at CRC.

1.3. Thesis Contributions

The goal of this thesis is to study manufacturing methods that are available to produce polymers, concentrating on those available at Draper, and down-select to determine the best method for use in translational research. Thesis contributions are as follows:

1. **Determine which polymer manufacturing method for is best suited to develop and build rigid plastic parts for the translational research of a micro-fluidic cartridge:**
   Translational research requires parts that are consistently generated to tight tolerances and low cost to meet the quantities

needed for clinical trials. This thesis will study and determine the best method available at Draper to produce polymer parts, concentrating on methods that are best suited for translational research. It will then develop a liquid polymer molding process for a micro-fluidic cartridge case study and attempt to prove its effectiveness by implementing the process to produce the cartridges required for clinical trials. Implementation of the molding process proves the claims of this thesis by producing micro-fluidic cartridge parts for less than $5 per cartridge.

2. **Develop an analytical technique to determine the robustness of the selected liquid polymer molding method and provide feedback on the expected quality of parts for a micro-fluidic cartridge:** The selected method for manufacturing uses a hand-held injector to supply liquid polymer into a mold cavity. Variable, user-controlled injection rates were studied to provide feedback on part design and enable robust part production. Using experimental data of injection rates, an analytical technique was developed to evaluate the polymer processing. The technique was then implemented to modify the design and processing of the micro-fluidic cartridge parts. After redesigning the cartridge parts based on analytical results, parts were successfully made using the liquid polymer molding method described in Chapter 2.

1.4. Thesis Overview

The remainder of this thesis is divided into three chapters.

Chapter 2 will provide details about the cartridge design and then proceed to discuss different manufacturing approaches considered for this application and detail the down-selection process. It will discuss details of the selected process and difficulties encountered with this process then proceed to discuss solutions to those problems and how they are applicable to scaling up production.

Chapter 3 will discuss the development of a simplified computational tool used to analyze the selected manufacturing method and how it influences process and design parameters. It will also discuss how this method was validated and how it was used to provide feedback for the development of the process discussed in Chapter 2.

Chapter 4 concludes the thesis by recapitulating the results of the process and analytical tool development. It will also discuss how the results of this thesis might impact other researchers undergoing translational research.

2. Manufacturing Process Selection & Development

2.1. Cartridge Design Details

The micro-fluidic cartridge used in this case study consists of an assembly of five rigid plastic parts with an array of 192 capillary tubes running through them and rubber seals on either side of the rigid plastic as seen in Figure 1 and Figure 2. The assembly of rigid plastic parts, shown in Figure 3, consists of two different part designs, repeated to create a subassembly.

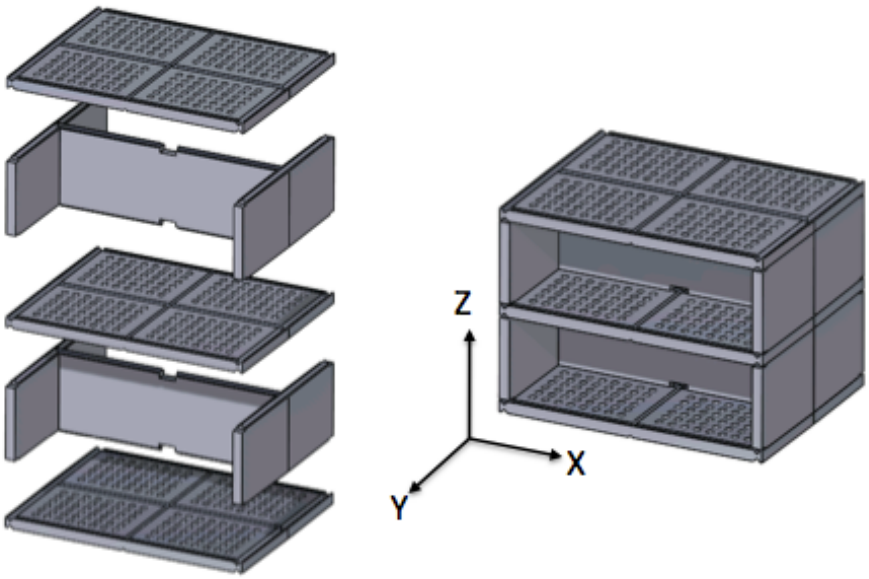

Figure 3 - Rigid Plastic Subassembly

The first of these two parts is an array plate that holds the capillary tubes in their planar (X-Y) position. The *Array Plate* (shown in Figure 4) has 192 through-holes to allow the tubes to pass through. These holes are sized slightly larger than the outer diameter of the capillary tubes (1.5 millimeters) to allow them to slip through without a press-fit. The holes are arranged in four quadrants with each quadrant containing forty-eight holes in a six-by-eight rectangular array. Each hole in a quadrant is offset from the neighboring hole by 2.25 millimeters. Triangular grooves, designed to provide mating alignment with adjacent parts of the cartridge assembly, are placed around the hole-array quadrants. The grooves exist on both sides of the array plate, making it symmetric. This is due to the design using three array plates separated by two lateral walls per assembly, therefore the center array plate is required to mate properly on both sides. The symmetric nature of this plate also makes the part bidirectional during assembly.

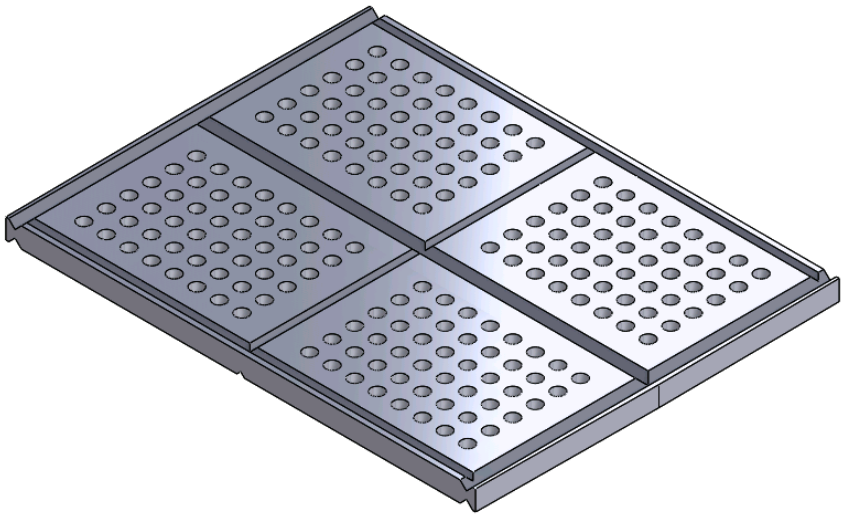

Figure 4 - Array Plate

The second part, the lateral wall, is an I-beam structure as shown in Figure 5. This part provides separation between the array plates to give the cartridge its appropriate Z-axis height allowing the cartridge to fit the required length of each capillary tube. Each lateral wall in an assembly mates to an array plate on either end and each has triangular bosses on either end to provide alignment. The lateral walls are also designed symmetrically which means that they are also not directional when assembled.

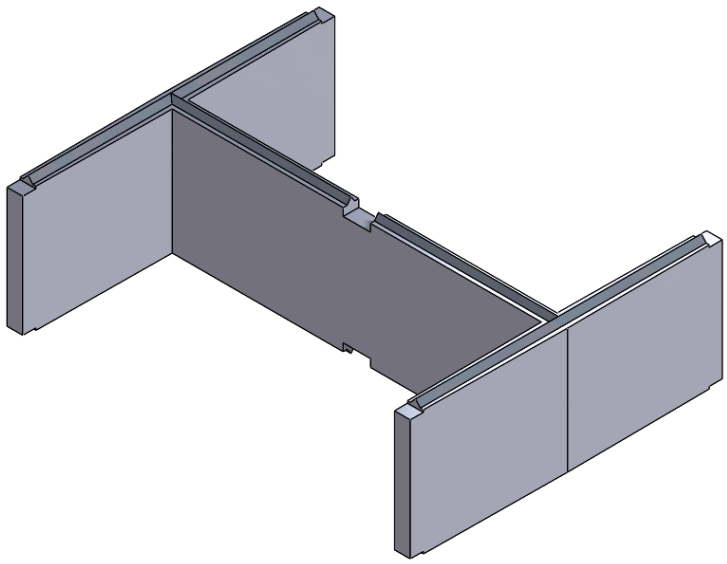

Figure 5 - Lateral Wall

At each end of the rigid plastic subassembly are silicone rubber gaskets used as a seal between the tubes and the fixture. On the upstream side of the cartridge is a single gasket that mates with the blood feed plenum. Downstream there are four separate gaskets to mate with the fixture. Both gaskets have through-holes to allow tubes to slip through. The holes are tapered so that at one end of the hole the diameter is slightly larger than the

tube outer diameter and the other end is slightly smaller than the tube outer diameter. This allows the gasket to easily slip over the tube for ease of assembly but also provides friction from the press-fit to hold the tube in place in the z-axis.

The capillary tubes for this micro-fluidic cartridge are commercial off-the-shelf (COTS) parts that are cut to 50 millimeters in length. Each tube has a 1.50mm outer diameter and a 0.30mm inner diameter.

2.2. Manufacturing Processes Investigation

Bench-top development of these micro-fluidic cartridges was performed at CRC where the rigid plastic components were made using three-dimensional (3D) printing and the gaskets were individually cast of silicone rubber.

To scale the production of cartridge parts, CRC partnered with Charles Stark Draper Laboratory (Draper) in Cambridge, Massachusetts to determine the appropriate manufacturing processes and build the cartridges required for clinical trials. Therefore, manufacturing processes considered for this project were limited to those available at Draper that include 3D printing, injection molding, standard machining, and reaction injection molding (RIM).

Construction of the gaskets needed to be outsourced since neither Draper nor CRC have the capability to efficiently create silicone parts at larger quantities. The initial method of casting the gaskets individually was determined to be too labor and time-intensive to be sustainable since casting

silicone rubber requires long duration cure times. The manufacturing process investigation was then limited to producing rigid plastic components.

2.2.1. Manufacturing Process Down-Selection

Machinists at Draper estimated standard machining of each part would cost greater than $10 per part for each array plate and lateral wall making each rigid subassembly cost $50. The alignment features would need to be redesigned using this process. In prototypes this feature was created using 3D printing, an additive manufacturing method, and cannot be easily replicated by machining thermoplastics, a subtractive manufacturing method. Direct machining is a poor candidate for production scale-up due to this high cost and minimal economics of scaling.

Cartridges used for laboratory testing at CRC were made using stereolitography (SLA), a particular type of 3D printing. It has already been established that parts created using SLA are too expensive to be used for larger quantities of parts. Although higher quantities using SLA would create some economics of scale, these savings are not enough to make the rigid parts at a suitable price.

The two remaining processes require a more detailed investigation to determine which is most appropriate.

2.2.1.1. Injection Molding

Injection molding is a method for processing large quantities of plastic parts. Thermoplastic pellets are melted and then injected into a metal mold containing a cavity with the part geometry. Part geometry needs to be considered since the molds are machined, a subtractive method of manufacturing, which, as stated above, cannot always create the same geometries as 3D printing. Another detail of this process to consider is the inclusion of draft angles for parts to release from the mold properly since the thermoplastic will shrink around mold features. This shrinkage creates large frictional forces that need to be overcome to extract parts from the mold.

Machined molds for injection molding are placed in a mold base, a standard piece of equipment for injection molding machines, which provides fluid lines into the mold to maintain the proper mold temperature. Mold bases also provide an ejector system that uses the hydraulics available in the molding machine to eject the plastic part after it has hardened [20]. The ejector system uses pins made of high strength steel that are ground to very tight tolerances in order to allow them to slip through holes in the mold cavity and release the part from the cavity.

Mold cavities are machined into mold base plates at tight tolerances to create the correct geometry and with fine surface finish to aid releasing parts from the cavity. Along with the design of the ejector system, this is an important feature of the mold as the part may become trapped in the mold as the

molten plastic shrinks when it cools. The need for fine surface finish indicates longer machining time and therefore higher mold cost. Molds intended for short-term use (short-run molds) would be appropriate for this application and can be made using easier-to-machine aluminum instead of steel. Aluminum molds can be machined faster than steel molds, providing some relief on machining time and cost [19].

Due to the use of high quality materials and tight tolerances required for mold bases, they add significant cost to any project. Commercial-off-the-shelf mold bases sized for the cartridge parts cost approximately $800 each. One mold base would be required for each part and would need additional machining to locate fluidic cooling paths and ejector pins. The mold for the *Array Plate* part would call for 192 pins (COTS ejector pins can be used), each costing approximately $20, in order to create the hole pattern. The molds also require precision machining in order to create both parts for the assembly. The combined cost for these molds is estimated to be $12,000, or $24 per cartridge (assuming 500 cartridges). A cost breakdown can be found in Table 1.

Table 1 - Mold Cost Breakdown, Injection Molding

Material/Process	Quantity	Subtotal (USD)	Total (USD)
Mold Base	2	$800	$1,600
Ejector Pins	200	$20	$4,000
Mold Cavity	2	$2,000	$4,000
Mold Base Machining	2	$1,200	$2,400
		Sum Total	$12,000

After the mold is machined, finished, assembled and fitted into the molding machine, initial molding trials begin. In many cases, initial parts are not built or do not perform as intend. If trial parts do not comply with their design, the mold may require rework. This process may be repeated until acceptable parts are generated [20]. Injection molding analysis tools exist to predict the placement of mold vents (designed to expel entrapped air from the mold cavity); predict flow paths in the mold; and predict other problems such as inadequate mold filling, warpage, and sink marks. Analytical tools may not be perfectly accurate which can result in a mold design that does not allow molten plastic to completely fill the cavity (short-shot) or may result in other potential molding problems. Additionally, injection molded parts greatly benefit from having near uniform wall thickness throughout to reduce residual stresses[20], which cannot be accomplished for the *array plate* as it is currently designed. The details described in this paragraph add significant technical risk to this method of manufacturing.

2.2.1.2. Reaction Injection Molding

Reaction Injection Molding (RIM) is a process where two liquid polymer components are injected into a cavity and a chemical reaction causes to components to crosslink resulting in a solid plastic part. Materials that can be Reaction Injection Molded are typically polyurethanes where the two liquids are isocyanate and polyol, or dicyclopentadiene [21]. Although the RIM process is often used in large-scale industrial applications using molding machines, the process can be modified for small-scale applications to be performed in a laboratory setting.

When used in large-scale operations to create large parts the RIM process relies on industrial molding machines that can handle large molds and large volumes of polyurethane. This industrial process is often used to produce large sandwich-like structures with nonporous skin and a porous, lower density core [22]. A diagram of an industrial RIM machine is shown in Figure 6. The use of these machines and molds adds significant overhead cost to part production. Using this process in a laboratory setting requires some modifications to the mold tooling and equipment; these modifications will be discussed later in this chapter.

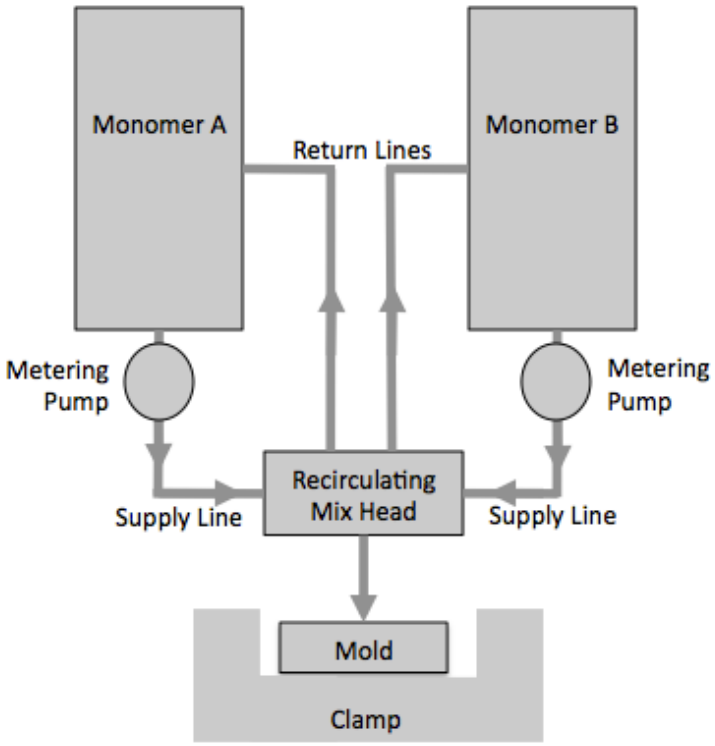

Figure 6 - Industrial Reaction Injection Molding Machine Diagram

The general advantage to using Reaction Injection Molding over standard Injection Molding is the use of lower viscosity materials for injection. The lower viscosity requires less injection pressure and therefore less clamp force to keep the mold closed during injection and prevent mold flashing. This lower clamp force does not require hydraulic clamping. The lower clamp force also does not require the use of expensive, machined tooling and therefore the time to create tooling can also be reduced. RIM parts have minimal shrinkage giving them good dimensional stability and the materials used provide good chemical resistance.

Disadvantages of this process include the processing time for each part to cure in the mold, limited materials selection, and inability to recycle used

material. Lastly, the raw materials for reaction molding are typically more expensive than those used for injection molding.

2.2.2. Manufacturing Process Selection for Micro-fluidic Cartridge

After comparing the processes available at Draper Laboratory to produce the Micro-fluidic Cartridge, it was decided to take the Reaction Injection Molding approach. This decision was based on the lower technical risk, as well as reduced cost and tooling time in order produce prototype parts to test with existing fixtures and methods. The Clinical Research Center at MIT also did not have an immediate need to obtain all of the cartridges at once that allows them to absorb the increased processing time of each individual cartridge. Lastly, the volume of material needed for each cartridge (15 ml/cartridge) is low so the cost of raw material becomes less significant than the cost of tooling for the quantities required to perform clinical trials. An estimated cost breakdown for the RIM molding to generate 500 cartridges can be found in Table 2. The combined cost for this process is approximately $2,030, or $4 per cartridge (assuming 500 cartridges).

Table 2 - Cost Breakdown, Reaction Injection Molding

Material	Quantity	Subtotal (USD)	Total (USD)
Rapid Prototype Mold Masters	12	$30	$360
Mold Box	2	$600	$1,200
Mold Max 30 (Rubber)	3 Gallons	$100	$300
Smooth-Cast 300 (Polyurethane)	2 Gallons	$85	$170
		Sum Total	$2,030

2.3. Manufacturing Process Development for Micro-fluidic Cartridge

The RIM process was modified for use in the laboratory to generate parts for the micro-fluidic cartridge. Instead of creating molds using machined parts, the molds were generated using silicone rubber. To do this, mold masters were made using a three-dimensional (3D) printing process and then silicone rubber was cast around the mold masters to create a two-part mold. When the mold masters were removed from the silicone, a mold cavity remained, which could then be filled with a thermosetting polymer and allowed to cure. This method allows for the creation of multiple cartridge parts from a single silicone mold and does not require expensive machinery to create molds or to inject the molds with resin.

2.3.1. Concept Manufacturing Process Details

As discussed in section 2.1, the two parts are designed with alignment features on both sides since the cartridge assembly is a stack-up of repeating parts. This feature's geometry requires that they can be removed from the mold in the Z-axis as shown in Figure 7, otherwise the features will create undercuts in the mold making them difficult to de-mold from a two-part mold.

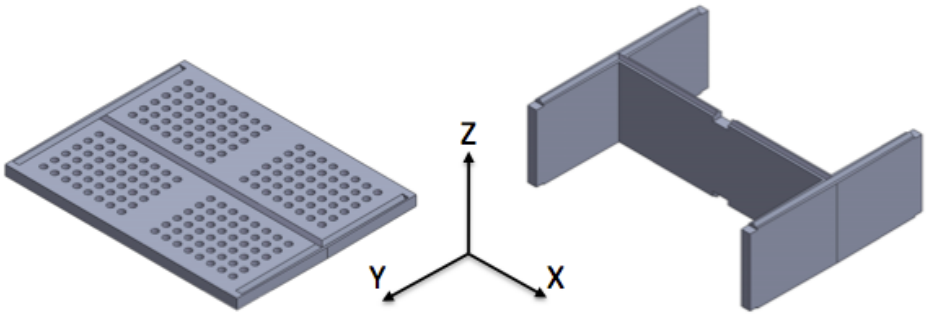

Figure 7 - Array Plate *and* Lateral Wall *with Reference Coordinates*

These two constraints require that the silicone rubber mold be split into two halves in order to maintain the alignment features on both sides of the molded parts. To do this, the mold masters must be placed in a mold box with one surface in contact with the box's bottom surface. The first silicone pour will then cover all of the part surfaces with the exception of the surface in contact with the bottom of the box. When the silicone is cured it can be removed from the well with the mold master encapsulated and still intact and then the other half can be molded. Prior to molding the second half, it is

necessary to use a mold-release agent or the second half will bond to the first, encapsulating the mold master parts prohibiting extraction.

2.3.1.1. Generating Mold Masters

The first step in Reaction Injection Molding using silicone molds is to generate mold masters. Three-dimensional printing was used as a quick and inexpensive method for producing the mold masters of the micro-fluidic cartridge parts. Three different 3D printing methods are available at Draper Laboratory: polyjet printing, fused deposition modeling (FDM), and stereo lithography (SLA).

Stereoliography uses a vat of photopolymer and a laser to cure the polymer. A platform in the vat moves deeper into the vat as each layer of the part is polymerized [23]. Due to the surface tension of the surrounding fluid, parts produced using SLA can be created with fine features accurate to their design geometry. For the mold masters, SLA was chosen due to its ability to accurately generate fine features and its minimal post-processing required for removing support material that is required during the SLA process. The ability to generate fine features was critical to create the triangular alignment features as well as for creating mold vent features that will be discussed in further detail in Chapter 3.

The use of 3D printing was also beneficial since prior prototypes were produced using this method so the creation of mold masters required

minimal design changes. In many instances, geometries that can be created using 3D printed cannot be produced using traditional machining such as square interior corners and the triangular grooves of the *Array Plate*.

One disadvantage to using 3D printing to generate the mold masters is the stepped nature in which 3D printed objects are created. This creates fine ridges in the finished part due to layer registration offsets in the SLA process. When these features are molded with silicone rubber, the rubber penetrates these ridges and acts as a mechanical lock to grip the mold master and any polyurethane parts that are subsequently molded into the rubber. In order to remove this effect, the surfaces that are built perpendicular to the printing direction need to be smoothed prior to molding into silicone. This processing step is critical in the holes of the *Array Plate* where the resulting silicone stems could easily tear off of the mold. The solution to this was to print the holes slightly undersized and then ream each hole by hand to the correct size.

Lastly prior to generating silicone molds, the mold masters must have mold release applied to them. This inhibits the silicone from creating a chemical bond to the mold master as well as generates a very smooth surface so that the silicone cannot make a mechanical grip to slight imperfections in the mold master.

To characterize and validate this process, a test piece was made of an *Array Plate* with the four quadrants of hole patterns treated differently, shown in Figure 8. The first quadrant was a baseline that was not reamed or coated

with mold release (Figure 8a); the second was only reamed (Figure 8b); the third was only coated with mold release (Figure 8c); and the fourth was reamed and coated with mold release (Figure 8d). The *Array Plate* was then molded with silicone and the mold master was removed from the silicone. Both of the hole patterns which were not reamed resulted in tearing silicone stems off of the mold. Although the section that was reamed without mold release did not tear any silicone, parts were significantly easier to extract from the section that was reamed and had mold release applied to it.

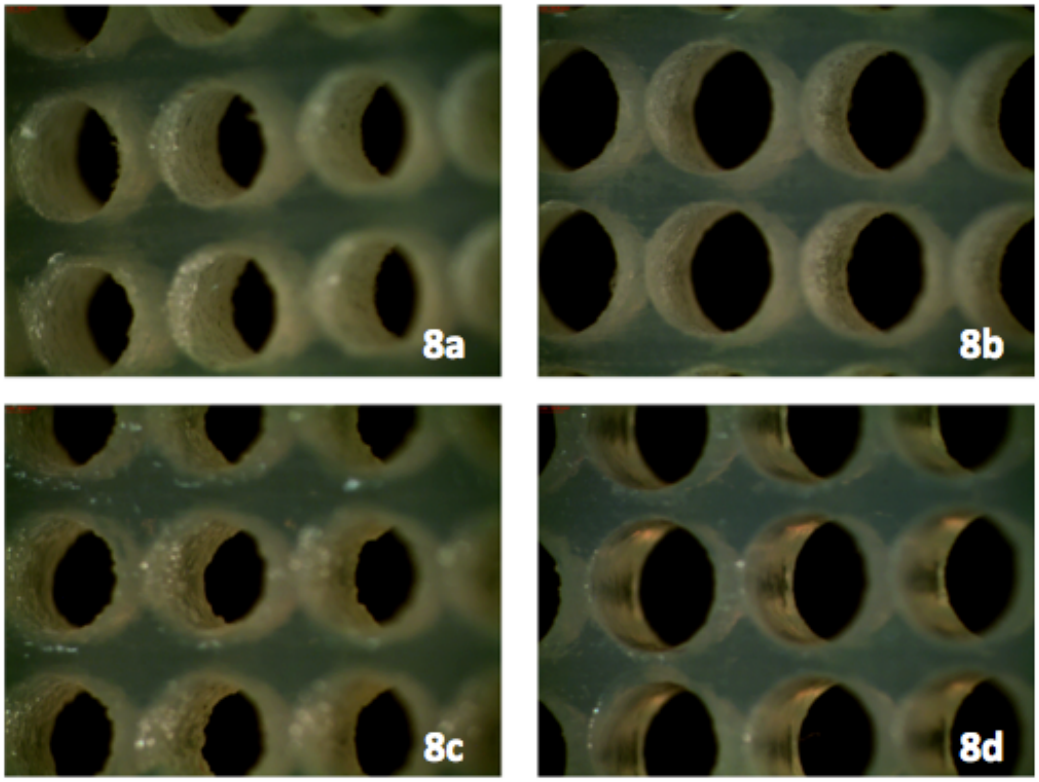

Figure 8 - Array Plate Hole Detail (2.0x Magnification)

2.3.1.2. Generating Silicone Molds

To generate the silicone molds the 3D printed mold master is first placed into a mold box to contain the silicone. For this application, Smooth-On Mold Max 30 was chosen as the silicone mold material given its relatively high tear-strength (125pli) while still being a low durometer (30 Shore A) which made extracting parts from the mold easier [24]. The two parts of Mold Max 30 are combined and degassed and in a vacuum at approximately -100 kPa (relative to atmosphere). The silicone is then poured into the mold box to cover the mold master part by at least 6 millimeters. The mold is then placed into a pressure vessel at approximately 600 kPa. This step ensures that no air bubbles remain in the silicone when it is cured and therefore exactly replicates the base 3D printed geometry.

After the first half of the mold is cured, the silicone and mold masters are removed from the mold box and inverted. Mold release is applied to all faces of the silicone to prepare it for the next pouring. This ensures that the next pouring of silicone does not bond with the first pouring, resulting in the inability to separate the two mold halves. The next step is to again mix the silicone, degass, pour into the mold box over the first mold half, and cure under pressure. When the second half of the mold is cured, the two halves can be separated and the mold masters can be removed from the mold. Smooth-On recommends post-curing the Mold-Max 30 four to six hours at

65°C for the silicone to reach final mechanical properties [24]. After post-curing the mold is ready for polyurethane injection.

In order for the two mold halves to align properly, a feature was added to the base plate of the mold box that creates a hemispherical boss on the first mold half. When the second mold half is molded over the first half, a hemispherical depression is generated. When the mold halves are recombined for injection the boss and depression features mate to ensure proper alignment. This alignment of the mold is crucial to ensuring that the triangular alignment features of the parts are in the proper relative positions on the top and bottom surfaces of the parts.

2.3.1.3. Injection

In order to properly fill the mold cavity the chosen polymer must be low viscosity so that it does not easily entrap air bubbles that will affect the final part geometry and to rapidly create parts it must also have a quick cure time. Lastly it should not react with the rubber mold material so that it bonds to the mold, which would severely shorten the life of the mold.

For this application, Smooth-On Smooth-Cast 300 was selected as the two-part urethane due to its low viscosity (80 cP) and its rapid cure time (10 minutes) [25]. It is also a good candidate material for this process since it uses a one-to-one by volume mixing ratio. The importance of mixing ratio will be discussed later in this chapter.

With the two mold halves assembled, the two-part polymer can be injected into the mold cavities. This can be achieved using a standard syringe of appropriate volume; however, the rapid cure time of the urethane limits the effectiveness of using a standard syringe since the material needs to be mixed prior to placing it in the syringe tube. The preferred method of injecting is to use a mixing syringe with static mixer tip.

A static mixer or motionless mixer is a device inserted into a housing or pipeline with the objective of manipulating fluid streams to divide, recombine, accelerate, spread, swirl or form layers as they pass through the mixer [3]. As a result of these alterations in the fluid flow, two separated fluids can be combined into one in a controlled and consistent manner. Due to the lack of moving parts, static mixers are an inexpensive method for mixing fluids without introducing air bubbles.

Prior to injecting the first part, a study was done to find a static mixer best suited for these parts. The best mixer should contain a low volume of material to minimize waste, be low cost, and mix the two components well enough to cure to hard polyurethane. Static mixers are specified by the number of elements, or layers, that the fluid distributes into to generate a fully mixed solution. Also, the selected injecting tool required the mixing tip to be a bayonet-style in order to mate properly with the tool. Lastly, two different types of static mixers exist, helical and square mixers, a photo of the filament from both styles of static mixer can be seen in Figure 9, and a static

mixer mounted on a mixing cartridge and loaded into a hand-held dispenser is show in Figure 11.

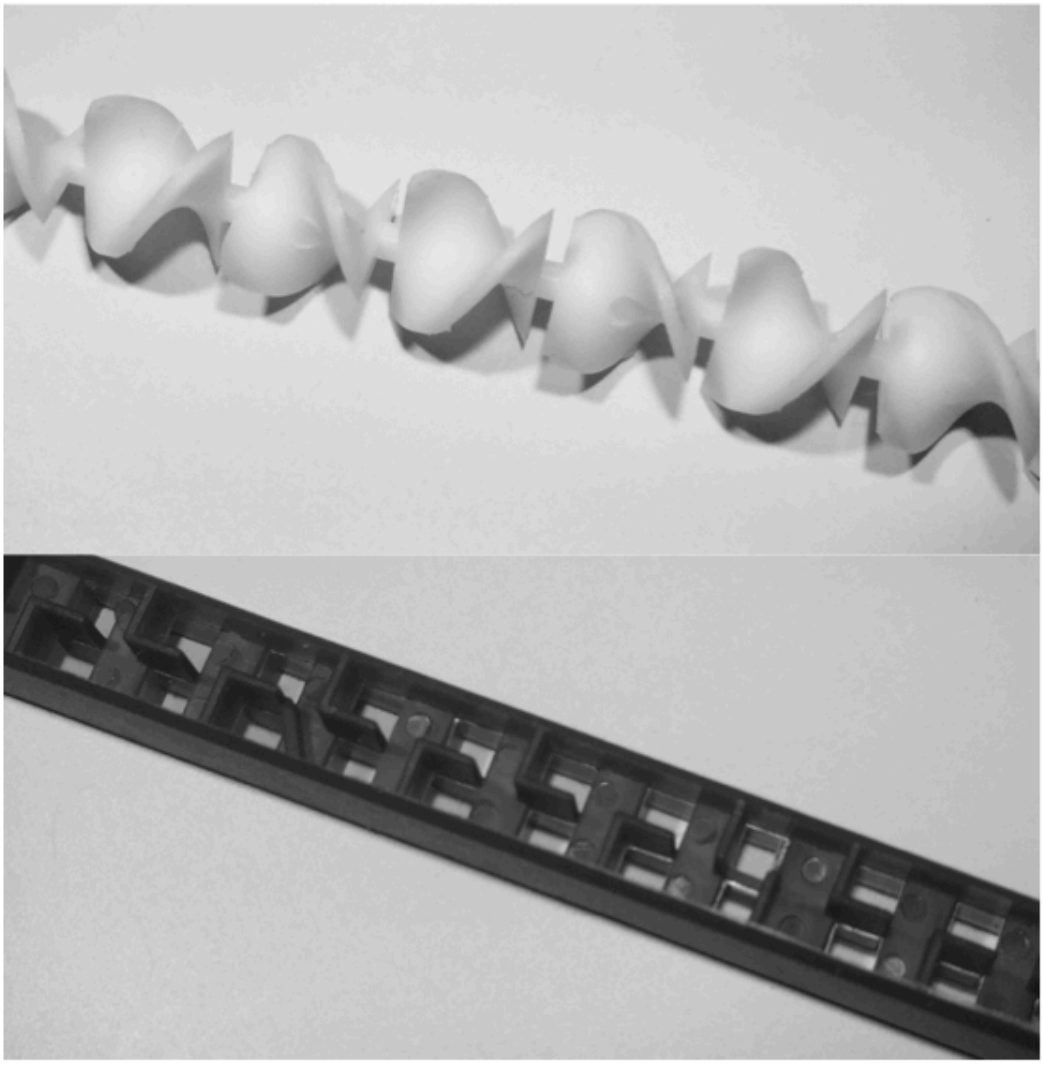

Figure 9 - Static Mixer Filaments

Multiple different static mixers were tested with the Smooth-Cast material ranging from seven elements to thirty-two elements; the table below describes the mixers.

Table 3 – Static Mixer Comparison

Number of Elements	Length	Diameter	Manufacturer and Part Number	Cost (per static mixer)
7	33mm	2.54mm	Sulzer EA3.0-07SA	$1.90
17	63.5mm	2.54mm	Sulzer EA3.0-17SA	$0.62
21	151.4mm	6.35mm	Sulzer EA6.3-21LA	$0.81
24	115mm	5.3mm	Sulzer EA300-026	$0.81

Of the four different static mixers tested, only the last two (EA6.3-21LA and EA300-026) mixed the material well enough for it to cure properly. The Sulzer EA300-026 is a square mixer which allows it to fit more elements in a shorter length. Due to its smaller size and therefore reduced waste material it was selected for the injecting process.

After the static mixer was selected, the two parts of the Smooth-Cast 300 polyurethane were placed into a two-part mixing cartridge with a one-to-one volume ratio as shown in Figure 10. The mixing ratio is important as cartridges come in even sizes such as one-to-one and two-to one. After placed in the cartridge the separated fluids are degassed under vacuum at approximately -100 kPa (relative to atmosphere) to reduce the amount of air bubbles trapped in the fluids. When degassing is completed, the cartridge is

assembled with plungers and loaded into a hand-held dispensing gun and a static mixer is attached to cartridge, shown in Figure 11.

Figure 10 – One-to-One Mixing Cartridge

Figure 11 – Hand-Held Dispensing Gun with Cartridge and Static Mixer

Variation is introduced in the process with the use the hand-held dispenser that can generate inconsistencies (i.e. air pockets) in parts produced. The one key variable is the rate at which fluid is injected; however, parts and molds

can be designed in a way to handle these variations, while still allowing consistent mold filling and part production. Such process robustness is essential to efficient production of low-cost, quality parts - the central goal of this thesis. This concepts will be further explored in Chapter 3.

2.3.1.4. Part Extraction

After the injected polyurethane is allowed to cure in the mold it can be extracted. The recommended cure time for Smooth-Cast 300 is ten minutes. At this time, the part is still pliable and can be plastically deformed when extracted from the mold. To accelerate this process the curing cycle can be performed at elevated temperature, approximately 65°C. After the initial cure the mold should be opened and allowed to cure for an additional ten minutes at 65°C so the material may harden. Once hardened the parts may be extracted from the mold without plastically deforming. After extracting parts from the mold, the parts should be post-cured at 65C for an additional four hours. Parts may be batch processed through this post-cure step that allows the material to obtain its final material strength and hardness.

2.3.2. Mold Details

This section will discuss details of the molding process regarding mold venting and mold clamping.

2.3.2.1. Mold Venting

Mold vents are a critical feature of the mold that allows air from the mold cavity to escape as the mold is being filled with resin. Vents need to be located on external surfaces or edges of the part and must provide a path for air to escape to atmosphere surrounding the mold [26]. Typically mold vents are located at the highest point of the mold so gravitational effects keep the resin at the bottom of the mold and the trapped air is gradually pushed towards the vent; however with the flat geometry of the array plate a high point does not exist.

To begin with, the initial mold vents for the array plate were located at each corner of the part with the injection gate located at the center of the plate. Vents and injection gates were initially created by using a hole punch to cut through the silicone mold; however, to obtain better precision for the location of these features they were later generated by placing thin posts on the 3D printed mold master. Due to flow restrictions around the patterned hole geometry, the fluid fills from the center inlet to the edges (shown in Figure 12) of the hole arrays before completely filling between the holes creating an air trap.

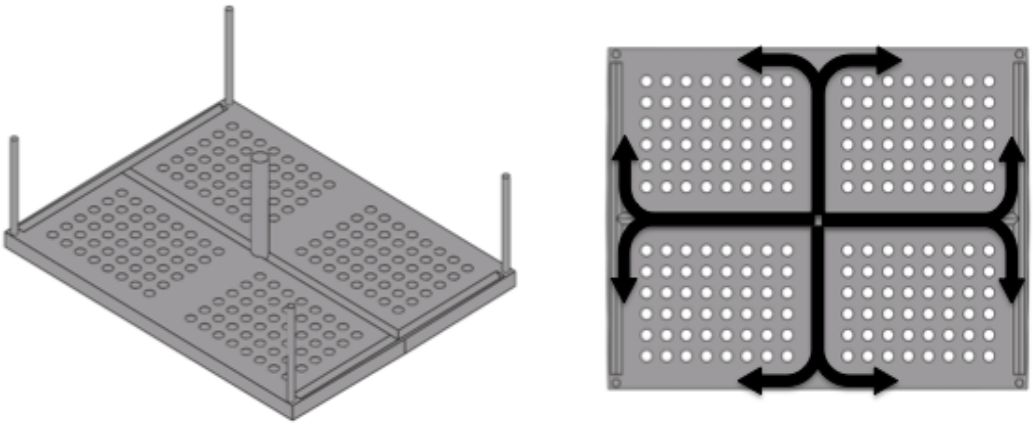

Figure 12 - Array Plate Gate and Vent Locations, Edge Flow Diagram

The next step was to place a new vent in the approximate center of the void left by the trapped air. Upon molding the geometry again, this time with eight vents, a void still consistently remained in the injected parts. Again, another new vent was placed in the approximate center of the remaining void. With twelve vents in the initial prototype mold, the parts were consistently filled without voids.

Vents were also needed in the mold for the lateral wall parts and again these vents were placed in the four corners of the geometry on the top edge as shown in Figure 13. The injection gate was placed in the center of this part and with this gate location the vent locations turned out to be the only ones necessary in order to completely fill the mold.

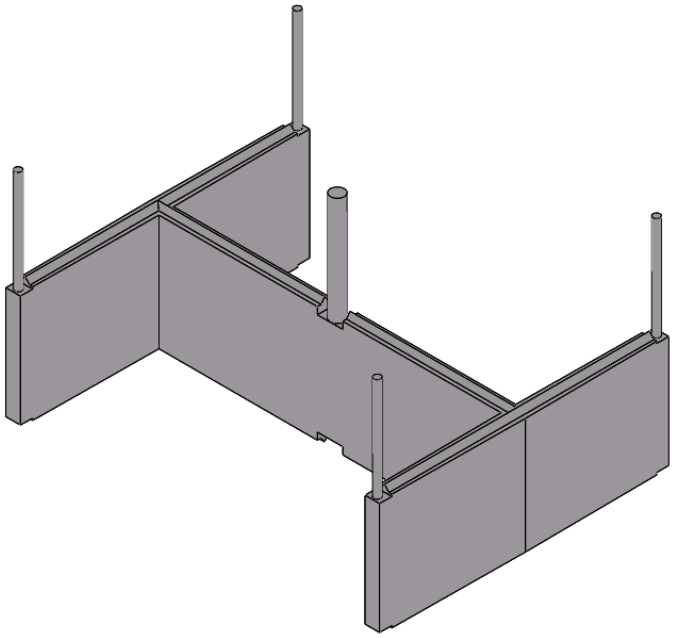

Figure 13 - Lateral Wall Gate and Vent Locations

In the RIM process, resin will flow through the mold vents and will require a post-processing step to remove the vent flashing. To maintain a minimal post-processing time it is necessary to use the minimum number of vents possible. The small diameters of the vents and injection sprues in both the array plate and lateral wall allow the user to remove these features by hand. A benefit of the mold vents filling with resin is that they provide visual feedback to the user when the mold has completed filling. Due to the low viscosity of the fluid being injected there is very little pressure build-up in the mold and the only feedback to indicate that the mold has filled is the visible fluid exiting through the vents.

Complex geometries such as the array plate are common in molding processes and the internal mold flows can be difficult to anticipate. While

mold venting in such cases can be done iteratively through trial and error, we felt it important to have a tool that helped predict vent placement for laboratory-scale RIM processing. Chapter 3 of this thesis will discuss an analytical modeling method that was developed in order to help determine vent locations.

2.3.2.2. Mold Clamping

One effect of injecting the fluid into the mold cavity is the propensity for flashing. Flashing occurs when the pressure inside the mold cavity exceeds the forces holding the mold halves together therefore allowing a thin layer of fluid to escape the cavity. When that fluid cures, a thin layer of polyurethane remains and must be trimmed from the remaining part, this thin layer is called flashing. A clamp frame was created to hold the mold halves in intimate contact while the mold cavity was injected to avoid flashing when using the silicone molds. The clamp consisted of two aluminum plates clamped around the exterior of the silicone mold using ¼-20 UNC bolts. Due to the low pressure in the mold during injection these bolts only need to be fastened "finger-tight" to provide adequate clamping. One clamp plate per mold contains pockets to prevent blocking mold vents and gates.

2.3.3. Micro-fluidic Cartridge Production Scale-Up

To scale up the production of parts to meet the needs for clinical trials multiple larger molds capable of injecting and curing numerous parts at a

time were needed. The first task in scaling up for production is to determine the number of mold masters that will be needed. The number of mold masters is based on the total number of cartridges needed and the time it will take to produce that quantity based on a few assumptions. The other factor in determining the amount of mold masters to create is determining a reasonable number to have 3D printed. Since much of the 3D printing cost for these parts lies in the set-up of the 3D printing machine it was determined the best approach would be to limit the quantity to what would be available in one run of the 3D printer. Based on the planar area of the printer (645 cm^2); the planar area of the parts (17.35 cm^2); and an assumed packing efficiency in the SLA machine of 75%, one run of the 3D printer would be able to produce approximately 27 parts.

Another approach is to create a single mold and uses parts generated by this mold as mold masters for other molds. This method saves money by reducing the need for rapid prototyped parts and the post-processing required for the parts discussed in Section 2.3.1.1.

Another consideration when making larger molds is the possibility for a mold to fail or deteriorate over time. With this in mind, it was decided to split the scaling of each part into multiple molds. However, when using multiple molds the processing time increases slightly as it takes time to clamp and unclamp the molds, as well as align each mold in the clamps. After considering these factors it was decided to print eight mold masters with the

intent of using six per mold. This would provide spare rapid prototype parts should one break during processing. Using the first mold to create three more molds would result in four molds for each geometry. If a cycle time of approximately 30 minutes is assumed per mold that includes mold setup, injection, curing, post-curing, and extraction, and assuming multiple molds can be done in parallel, it is estimated to take approximately 33 hours of molding in order to produce enough parts for 500 cartridges.

Clamping was revisited when scaling up the molds to have six cavities per mold. Since the clamp plates are created from one sheet of aluminum plate requiring pockets to allow mold gates and vents access to atmosphere, the mold cavities will need to be spaced in a controlled manner so the mold gate and vents align with pockets in the clamp plate. A locating plate was created to maintain proper spacing between each mold master. This locating plate uses six pockets milled to the same depth that mate on the vent and gate pins of the 3D printed mold master. Another feature of the locating plate are large holes that allow the silicone to be poured through the plate in order to fully cover the mold master parts as the locating plate remains in place during silicone pouring and curing. The locating plate and mold masters are placed in a mold box and silicone may then be poured to generate the first mold half. After the first mold half has cured, the spacing of the mold cavities is set and the locating plate is no longer necessary for molding the second half.

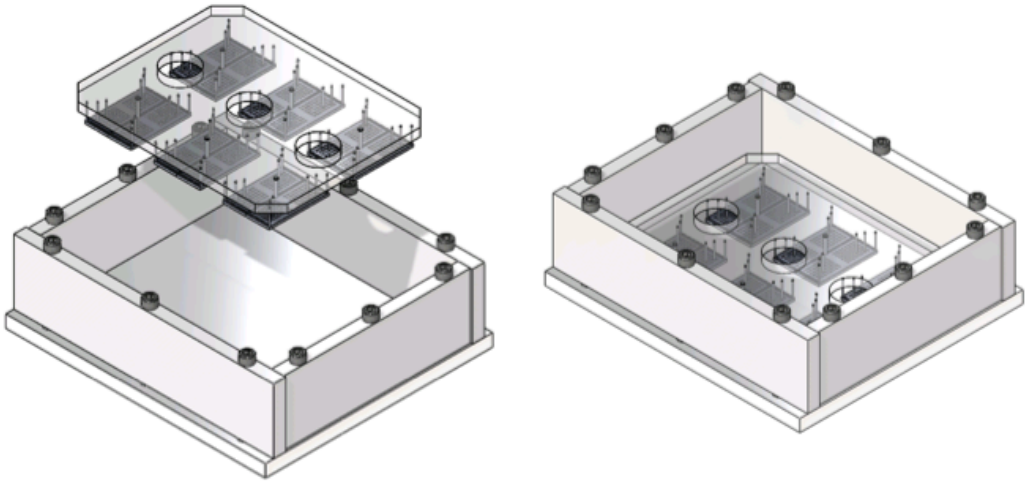

Figure 14 - Mold Masters and Locating Plate, Outside and Inside Mold Box

2.4. Discussion and Next Steps

This process has proven to be successful at creating cartridge parts and scaling-up production is currently progressing. To measure how consistently this process produces parts, dimensions of the molded array plate parts were taken and compared to the dimensions as drawn and dimensions of the 3D printed parts. The printed parts provide a good baseline to measure molded parts against as the printed parts have proven to work through prototype, bench-top testing at CRC. The dimensions used for comparison are shown in Figure 15 and include the overall length (l), overall width (w), thickness (t), hole diameter (d), and a cross-wise hole to hole dimension (a). Five molded parts and five 3D printed parts were measured to provide a range of dimensions and allow us to estimate tolerances for the parts. The measurements and their estimated tolerances (in parenthesis) can be found

in Table 4. The calculated tolerance value represents the difference of maximum and minimum values from the average dimension, which was taken to represent a nominal dimension.

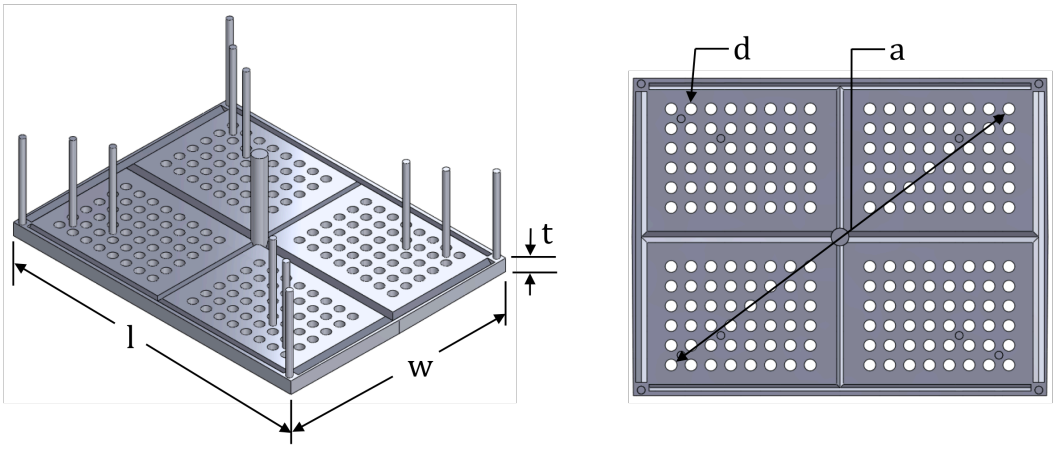

Figure 15 – Array Plate Dimension Designations

Table 4 – Array Plate Dimensions, Measured

Dimension	As-Drawn (mm)	3D Printed Part (mm)	RIM Part (mm)
l	47.14	47.17-47.31 (±0.07)	47.03-47.17 (±0.07)
w	36.25	36.26-36.33 (±0.04)	36.10-36.13 (±0.02)
t	2.00	2.17-2.33 (±0.08)	2.23-2.34 (±0.06)
d	1.35	1.08-1.18 (±0.05)	1.50-1.54 (±0.02)
a	46.81	46.95-47.05 (±0.05)	46.55-46.64 (±0.05)

The differences between printed and molded parts in the length and width dimension are attributed to shrinkage in polyurethane material as it cures.

Although the magnitude of these dimensions may differ, the tolerances of each method are similar. The most noticeable difference in tolerance occurs in the hole diameter where the 3D printed tolerance is more than two-times that of the RIM part. This is due to the reaming process used for making the mold masters in Reaction Injection Molding.

Future work can proceed by investigating larger quantities of parts to obtain statistical significance and in particular how the Reaction Injection Molding method functions over time. Evaluating part dimensions and tolerances over time will determine if and when silicone molds deteriorate to a point where they are no longer consistently generating useful parts.

2.5. Summary

This chapter discusses the down-selection process for determining which manufacturing method is best suited for the production of rigid plastic parts for a micro-fluidic cartridge. It concludes that reaction injection molding is the method best suited for this application in order to advance the micro-fluidic cartridge to clinical trials. Details of this method are discussed that include generating mold masters; creating silicone rubber molds; injection of a polyurethane; mold venting; and mold clamping. In addition, methods are discussed for scaling the process to meet the clinical trial demand of multiple-hundred assemblies.

The reaction injection molding process was selected and implemented. It allows us to consistently build micro-fluidic cartridge parts using silicone rubber molds and a hand-held injection tool. The silicone molds were pressure cast around rapid-prototype mold masters. Using the techniques described in this chapter for scaling up production, the rigid plastic subassemblies for the micro-fluidic cartridge are produced for approximately $4 each. The consistency of parts being built with this process is demonstrated through the tolerance analysis comparing molded parts with printed parts that have been proven to work in bench-top testing.

3. Computational Analysis using the Finite Element Method

During the injection process described in section 2.3.1.3, the two-part polyurethane fluid flows into the mold cavity, and in doing so it replaces atmospheric air. If the mold is not vented properly the fluid may separate and recombine in the cavity leaving trapped volumes of air. These air traps will affect the final molded geometry and may affect the part's functionality.

This chapter will discuss a simplified, computationally efficient method for simulating fluid flow in the mold cavities of the cartridge parts. Simulations will account for variance caused by the human interaction during injection to determine how robust the part design is to variations in injection flow rate. The purpose of this simulation method is to determine where air traps occur during the injection process to aid in locating mold vents and allow us to redesign parts so they fill properly over a variety of injection flow rates. Using this analytical method, the cartridge parts were redesigned to ensure the molds would fill without voids.

3.1. Simulation Approach

The initial approach to solve for the location of air traps was to use the plastics processing analytical tool Solidworks Plastics, currently available at Draper. This is a finite element analysis tool designed for injection molding thermoplastic that solves for air traps, among other factors. As a thermoplastics analytical module, it requires input parameters that do not pertain to thermosets, such as the material melt temperature, and it also requires material information that is not supplied for Smooth-Cast 300 such as the specific heat, thermal expansion coefficient and thermal conductivity. Since these parameters are not provided for the Smooth-Cast 300 resin and the Solidworks Plastics software is tailored to simulate the thermoplastic injection molding process, we decided to take a different approach to solve for air traps that occur during the RIM process.

The simulation approach we used is a fluid flow analysis coupled with a species convection-diffusion model using *COMSOL Multiphysics.* Although this technique does not model the physics of what is occurring during the injection process (i.e. the injection of liquid into an initially gas-filled chamber), we hypothesized that we could approximate the solution for the liquid-gas interface between the resin and air in the mold cavity by using this approach along with experimental results of the filling process. The time-dependent concentration solution in the simulation will be used to approximate the liquid polymer flow front; that is, the polymer-air interface.

Higher concentrations estimate where the polymer is in the model and lower concentrations estimate the volume of air remaining in the model. Due to its complex nature in regard to fluid filling, the *array plate* was the basis for simulations; however, the *lateral wall* is also simulated.

Generally, mold filling can be complex to model as a chemical reaction and phase change are taking place. In the RIM process, an exothermal reaction occurs and the viscosity of the injection fluid increases as the polymer chains cross-link. Modeling techniques have been previously developed that take into account factors such as changing viscosity [28], changing fluid temperature, and use of structural fillers [29]. Due to the small volume of the individual cartridge parts and the short mold filling time, relative to the material curing time, it is assumed the material has not had enough time to cross-link to any meaningful extent. This assumption leads to two general assumptions aimed at simplifying our modeling:

1. The injection process is isothermal;
2. The viscosity of the fluid remains constant.

These assumptions are supported in texts by Russ, Castro, et al., and by J.W. Blake [27, 30, 31].

3.2. Simulation Development

The simulation model for the array plate was done as a quarter model using symmetry conditions in order to simplify each iteration and reduce the

amount of computation time. In order to further simply the simulations the triangular alignment grooves were removed for initial analytical iterations. Figure 16 below shows the full-scale model of an array plate as well as the corresponding one-quarter model depicting the direction of fluid flow at the inlet and at each vent. The flow is prescribed at the inlet by an average velocity across the inlet surface. A fixed back-pressure (atmospheric pressure) is prescribed at each vent outlet. The two surfaces of symmetry are noted in Figure 16 and the remaining surfaces are prescribed a wall boundary condition.

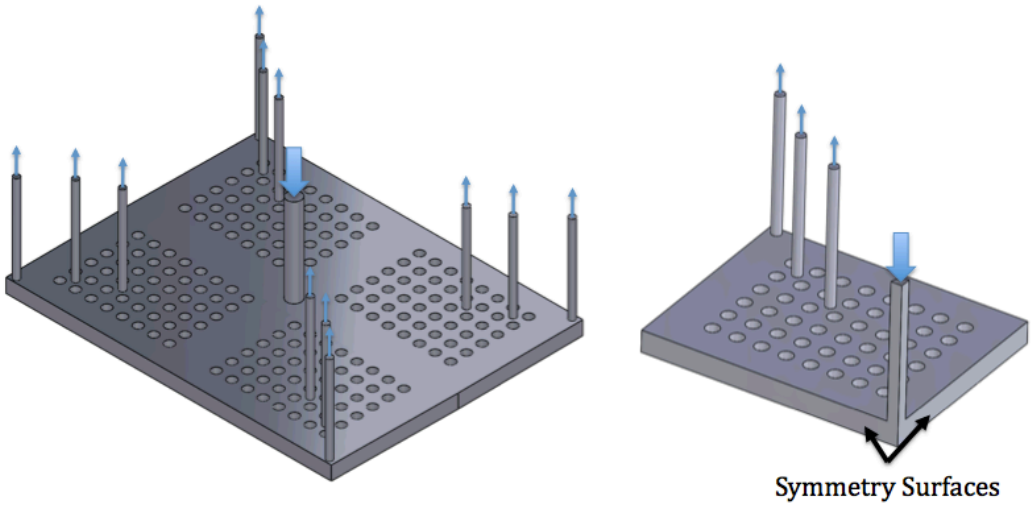

Figure 16 - Full Scale Model and Reduced One-Quarter Model

To generate a baseline analytical method the array plate was simulated with both eight vents and twelve vents. Each was validated by comparison to video recordings.

3.2.1. Governing Equations

The simulations are based on a fluid flow analysis that are governed by the Navier-Stokes equations, which in their general form consist of the continuity equation:

$$\frac{\partial \rho}{\partial t} + \nabla \cdot (\rho \mathbf{u}) = 0 \qquad [1]$$

and the momentum equation:

$$\rho \frac{\partial \mathbf{u}}{\partial t} + \rho(\mathbf{u} \cdot \nabla)\mathbf{u} = \nabla \cdot (-p\mathbf{I} + \tau) + \mathbf{F} \qquad [2]$$

where ρ is the fluid density; μ is the fluid viscosity; τ is the viscous stress tensor; **u** is the velocity vector; t is time; *p* is pressure; **I** is the identity matrix; and **F** is the body force matrix.

For the simulations, it is assumed the inlet fluid velocity does not vary with time and flow throughout the model is steady, therefore:

$$\frac{\partial \mathbf{u}}{\partial t} = 0 \qquad [3]$$

The assumption of steady flow is supported by data from modeling iterations comparing steady and unsteady flow simulations that are described in Section 3.3.1 of this document.

This flow is also assumed to be incompressible and since the injection process is done in a thermally stable environment and the polymerizing reaction is assumed to be isothermal, as described in Section 3.1, all

temperature effects are assumed to be negligible. With these assumptions the continuity equation reduces to:

$$\rho\nabla\cdot\mathbf{u}=0 \qquad [4]$$

and the momentum equation reduces to:

$$\rho(\mathbf{u}\cdot\nabla)\mathbf{u}=-\nabla\cdot p\mathbf{I}+\mu\nabla^2\mathbf{u}+\mathbf{F} \qquad [5]$$

Lastly, the only body force to consider in this analysis is the force of gravity. However, the gravitational forces, calculated using the equation:

$$F=\rho g h \qquad [6]$$

where *h* is the height in the direction gravity is acting, are negligible relative to viscous forces. Therefore the final term of Equation 5 can be ignored resulting in:

$$\rho(\mathbf{u}\cdot\nabla)\mathbf{u}=-\nabla\cdot p\mathbf{I}+\mu\nabla^2\mathbf{u} \qquad [7]$$

The continuity and momentum partial differential equations are used in the finite element models to solve for the velocity and pressure in each element.

The convection-diffusion model is governed by the equation:

$$\frac{\partial c}{\partial t}+\mathbf{u}\cdot\nabla c=\nabla\cdot(D\nabla c)+R \qquad [8]$$

Where c is the concentration; D is the diffusion coefficient; and R is the reaction rate expression for the species.

Since this analysis is not concerned with chemical reactions, but rather the flow in the mold cavity, the reaction rate term from this equation is negligible and the equation simplifies to:

$$\frac{\partial c}{\partial t} + \mathbf{u} \cdot \nabla c = \nabla \cdot \left(D \nabla c \right) \qquad [9]$$

This partial differential equation uses the previously solved velocity as an input for each element and solves for the time dependent concentration. An initial concentration is prescribed at the inlet boundary while the remainder of the model has zero concentration. The inlet concentration then drives concentrations throughout the model based on the fluid flow solution.

3.2.2. Boundary Conditions and Initial Conditions

As discussed earlier in this chapter the *Array Plate* simulation was done with a symmetry condition, using one-quarter of the geometry. The *symmetry* condition was applied to surfaces two and three (Figure 17) for both *array plate* model types, eight-vent and twelve-vent. For the flow analysis, the symmetry condition prescribes no perpendicular flow penetration and vanishing shear stress along these surfaces. Mathematically, the continuity equation at the symmetry surface becomes:

$$\mathbf{u} \cdot \mathbf{n} = 0 \qquad [10]$$

and the momentum equation becomes:

$$\left(-\nabla\cdot\ p\mathbf{I}+\mu\nabla^2\mathbf{u}\right)\mathbf{n}=0 \qquad [11]$$

In the species transport model, the symmetry condition represents boundaries where there is no mass flux in the normal direction across the boundary. The equation that governs this condition is:

$$-\mathbf{n}\cdot\left(c\mathbf{u}-D\nabla c\right)=0 \qquad [12]$$

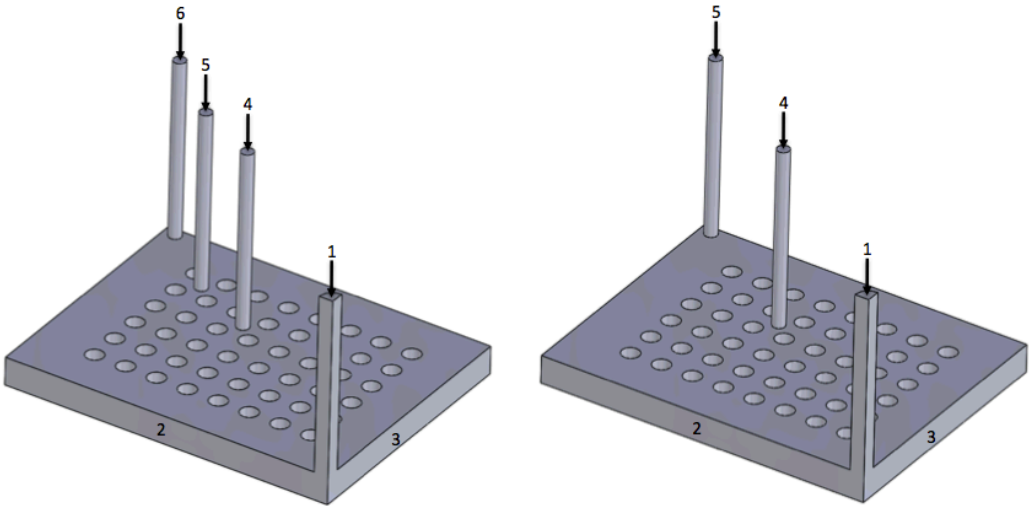

Figure 17 – Analytical Geometry with Surface Reference Numbers for the 12-vent case (l) and the 8-vent case (r)

Surfaces four through six in the twelve-vent case and surfaces four and five in the eight-vent case are assigned an *outlet* boundary condition, as this is where flow would exit. For the flow analysis, this boundary condition equates to a constant pressure condition, P_0, with no viscous stress. For these analyses P_0 was set to equal 0, which *COMSOL Multiphysics* interprets

as $P_{atm}+P_0$, where P_{atm} equals 1 atmosphere. For the species transport analysis, this outflow condition allows the species to transport through the boundary although it is assumed that convection is the dominating transport mechanism across the boundary and therefore diffusive transport can be ignored. That is,

$$\mathbf{n}\cdot\left(-D\nabla c\right)=0 \qquad [13]$$

Surface one for both geometries is the *inlet* for both fluid flow and the species transport analyses. For the flow analysis an average inlet fluid velocity, **u**, is prescribed. This boundary condition assumes fully developed flow and *COMSOL Multiphysics* adds an ordinary differential equation that calculates the pressure at the inlet such that the desired inlet velocity is obtained. The fully developed inlet velocity condition was used as opposed to a volumetric flow rate in order to avoid complications that would arise from assigning a flow entry length. Estimates for the average inlet velocities were obtained experimentally as described in Section 3.2.4.1 below.

For the species transport analysis a boundary condition for the concentration, c_0, is prescribed to the inflow surfaces (Surface 1). The convection-diffusion analyses only rely on a relative concentration, not absolute concentration, throughout the model and therefore an arbitrary value of 1 mol/m^3 was designated for c_0 at a t_0 value of zero seconds.

The remaining surfaces of the model were set to *no slip wall* conditions for the flow analysis and *no flux* conditions for the species transport. The no slip condition sets the fluid velocity equal to zero and the no flux condition creates boundaries where no mass flows in or out through the boundary, that is the flux is zero.

3.2.3. Meshed Model

Both geometries were meshed for the three-dimensional finite element model with approximately 150,000 elements in each model. The meshed models for the two geometries can be seen in Figure 18 and Figure 19.

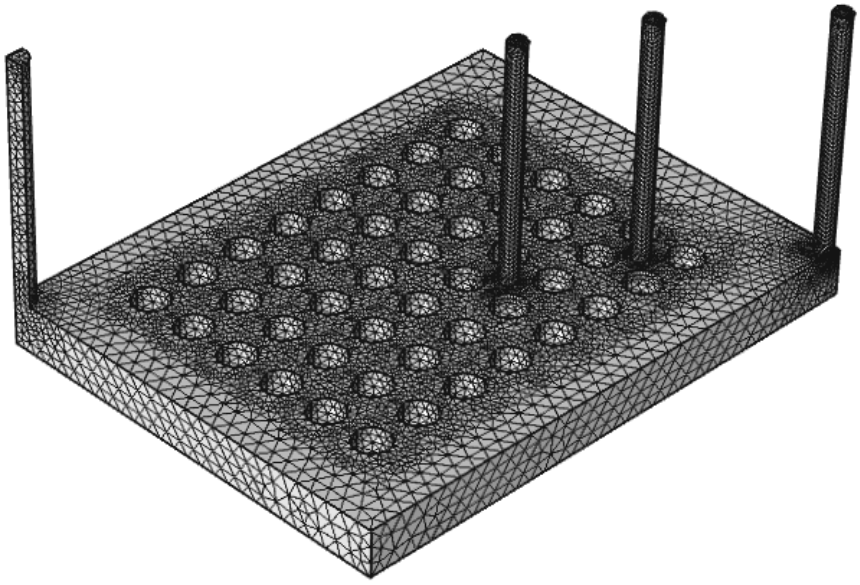

Figure 18 – Meshed Geometry, 12 Vent Case

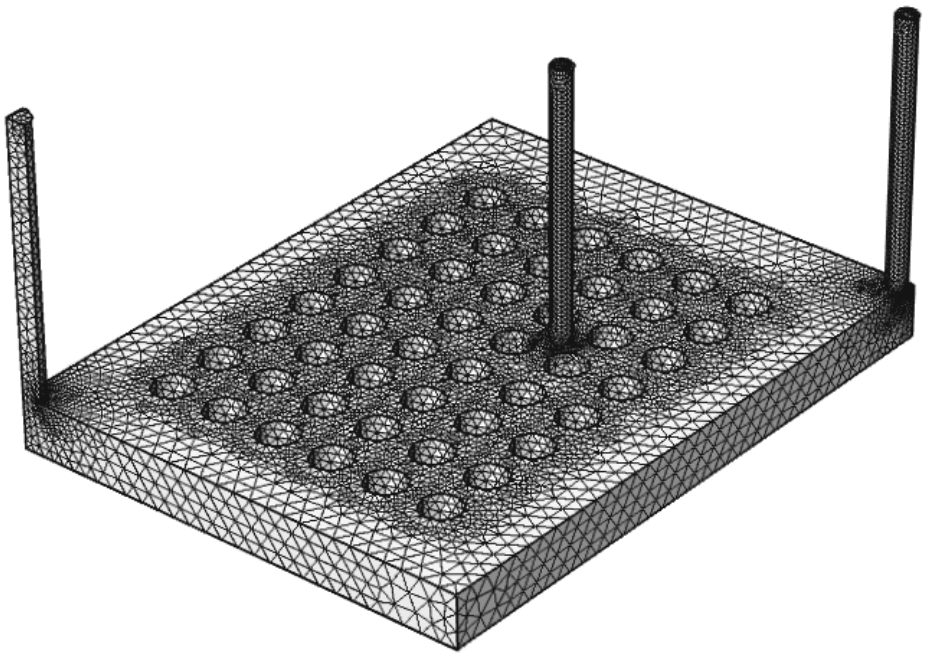

Figure 19 - Meshed Geometry, 8 Vent Case

3.2.4. Model Parameters

The constant needed to obtain the flow solution based on Equations 4 and 7, viscosity (μ) and density (ρ) are obtained from the material data sheet of Smooth-Cast 300. The values for each are:

$$\rho = 1080 \text{ kg/m}^3$$

$$\mu = 80 \text{ cps.}$$

The constant that is required to obtain a solution for the species transport model based on Equation 9 is the diffusion coefficient. Since the model is aimed at modeling the convective flow of the fluid, the diffusion coefficient is

set to a low value; however, a more exact value for the diffusion coefficient will be determined by comparing the simulation results to the experimental results. The process for determining the coefficient's value is described in Section 3.3.

3.2.4.1. Obtaining Fluid Flow Boundary Condition Input through Experimentation

Some model parameters could not be assumed and are not provided; therefore it was necessary to perform experiments in order to generate these input parameters. The model inputs for density and viscosity of the fluid are provided by the manufacturer (Smooth-On); therefore, the missing variable to solve the steady flow analysis is the inlet velocity. To study this, video was taken of the fluid injection and then post-processed to provide an estimate of inlet flow velocity.

Two prototype molds were generated to provide a fluid inlet velocity for the simulation as well as allow for validating the fluid simulation; one prototype with eight vents and another with twelve vents. As discussed in Section 2.3.2.1 a mold with twelve vents would consistently fill without trapped air, while a mold with eight vents would not. In order to create a complete comparison between geometries that both successfully and unsuccessfully fill the mold cavity, both were prototyped and tested with all other geometries equal between the two.

Using these prototype molds and aluminum clamp plates for a single cavity mold, experiments were run by injecting Smooth-Cast 300 into the mold cavities using a hand-held dispenser and a static mixer (Sulzer EA300-026). The molds were made of a translucent silicone and the Smooth-Cast 300 material was dyed black in order for it to be visible inside the mold cavity during injection. Both molds were injected at a variety of speeds to allow for the analysis of variation in the user controlled inlet velocity. Qualitatively the speeds were characterized as slow, medium-slow, medium-fast, and fast.

The injections were filmed at a frame rate of 29.95 frames per second and the output of the recordings was the frame number at the beginning of injection and the frame number at the end of injection, defined as the vents being filled with fluid. Constant mass flow rate was assumed and by using the volume of the cavity and the time to fill, an estimated volumetric flow rate was obtained for each injection. An average velocity at the inlet was obtained by dividing the volumetric flow rate by the inlet area. The velocities for each experimental case can be seen below in Table 5 and complete experimental video results can be found in Appendix A.

Table 5 – Injection Flow Rates

Mold Type	12 vents	8 vents	12 vents	8 vents	12 vents	8 vents	12 vents	8 vents
Qualitative Velocity	Slow	Slow	Med/ Slow	Med/ Slow	Med/ Fast	Med/ Fast	Fast	Fast
Velocity (m/s)	.102	.086	.176	.151	.183	.164	.538	.429

As seen in the above table the medium-slow and medium-fast velocities are relatively similar and will be referred to collectively as medium from this point on. These estimated velocities could now be used as inputs for the flow simulations.

3.3. Simulation Results and Post-Processing

This section will first discuss our initial flow results comparing steady and unsteady flows. It will then proceed to discuss the remaining simulation results and compare them to our video experimentation results.

3.3.1. Steady Flow Assumption Validation

Initially, the flow simulation was run as an unsteady model. This assumption requires significant computing resources and time as the flow and convection-diffusion model are both time-dependent and each must be solved at a number of time steps. A flow simulation of the array plate with eight vents was first run as an unsteady, time-dependent simulation. The velocity profile of the fluid can be found in Figure 20, with the injection location in the bottom left corner of each frame. The velocity profiles shown are taken at a mid-plane between the top and bottom surfaces of the array plate. As shown in this figure there is no discernable difference in the velocity profile at the varying time steps.

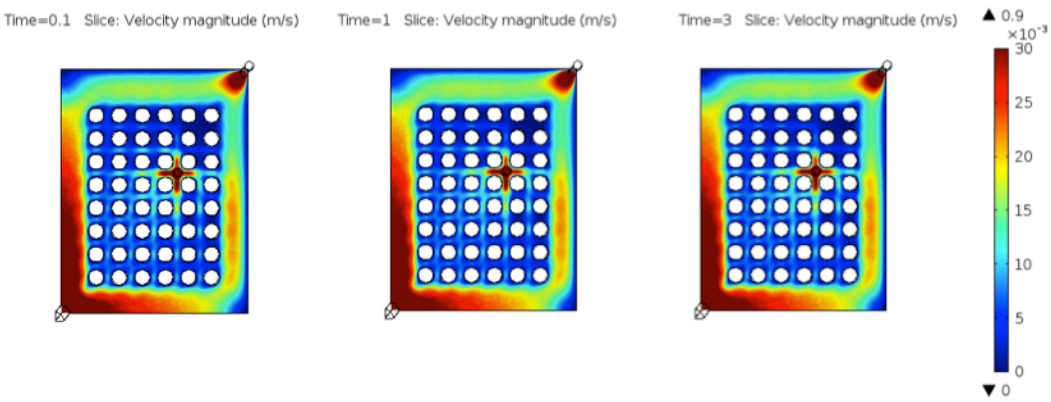

Figure 20 - Unsteady Flow Velocity Profiles (m/s), 8 vents, u = 0.429 m/s

For comparison, the simulation was run with the same boundary conditions as above with the exception that it was run as a steady flow simulation. The resulting velocity profile for this simulation is shown below in Figure 21.

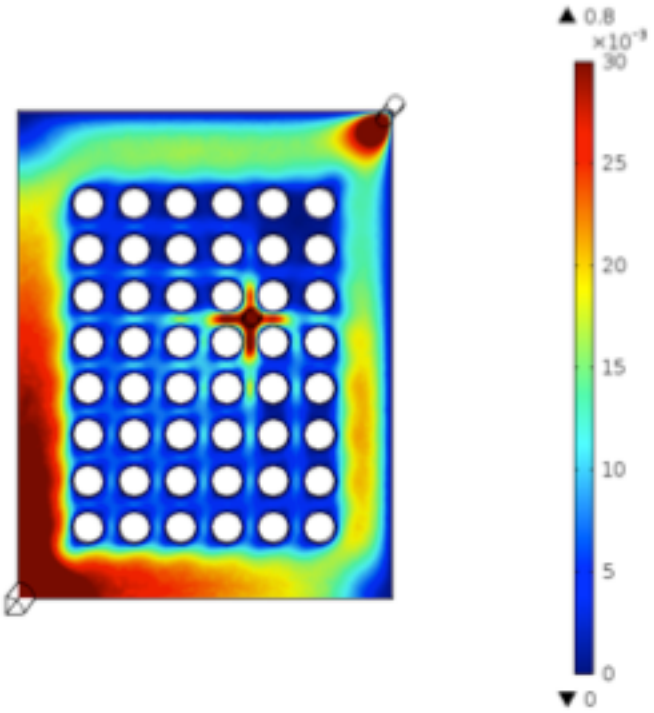

Figure 21 - Steady Flow Velocity Profile (m/s), 8 vents, u = 0.429 m/s

The color scales for the unsteady and steady flow velocities are matched and it is shown that these velocity profiles are identical. Therefore, going forward the simulations are run using steady flow to reduce computational time and the assumptions described in Section are valid.

3.3.2. Simulation Results and Validation

The remainder of this section will discuss the transient results of the combined fluid flow and convection-diffusion model and how the theoretical results compare to experimental results for two different geometry cases. It will also describe how the results lead to determining the proper diffusion coefficient for other simulation iterations.

The first case used to investigate the simulation results uses eight-vent geometry, shown in Figure 19, and a fast inlet velocity of 0.429 m/s. By monitoring the concentrations of the outlets over time it can be determined when the fluid is likely exiting the mold and mold filling is complete. After determining the filling time, quantification of the concentration throughout the part can be used to determine if the cavity is filled properly by observing the flow front defined by the concentration gradient. Regions that are green in the solution plots have filled with liquid polymer, regions that are red have not filled, and regions that are yellow may be filled. The eight-vent geometry and fast velocity were used since this condition consistently produced parts with voids caused by trapped air. The unfilled condition should leave a

distinctly low concentration (red) in the simulation results in the region where a trapped air volume was observed in the video analysis.

Video frames looking down on the mold for the 8-vent case at a high flow rate are shown in Figure 22. In the final frame (t = 3.40s) an air trap is seen between the vents in all four corners. This video was shot looking directly down onto the translucent mold and the static mixer nozzle can be seen at the center of each frame injecting the fluid through the inlet. The eight vent locations are also shown in the four corners of each frame, they are best defined in the final frame (t = 3.40s).

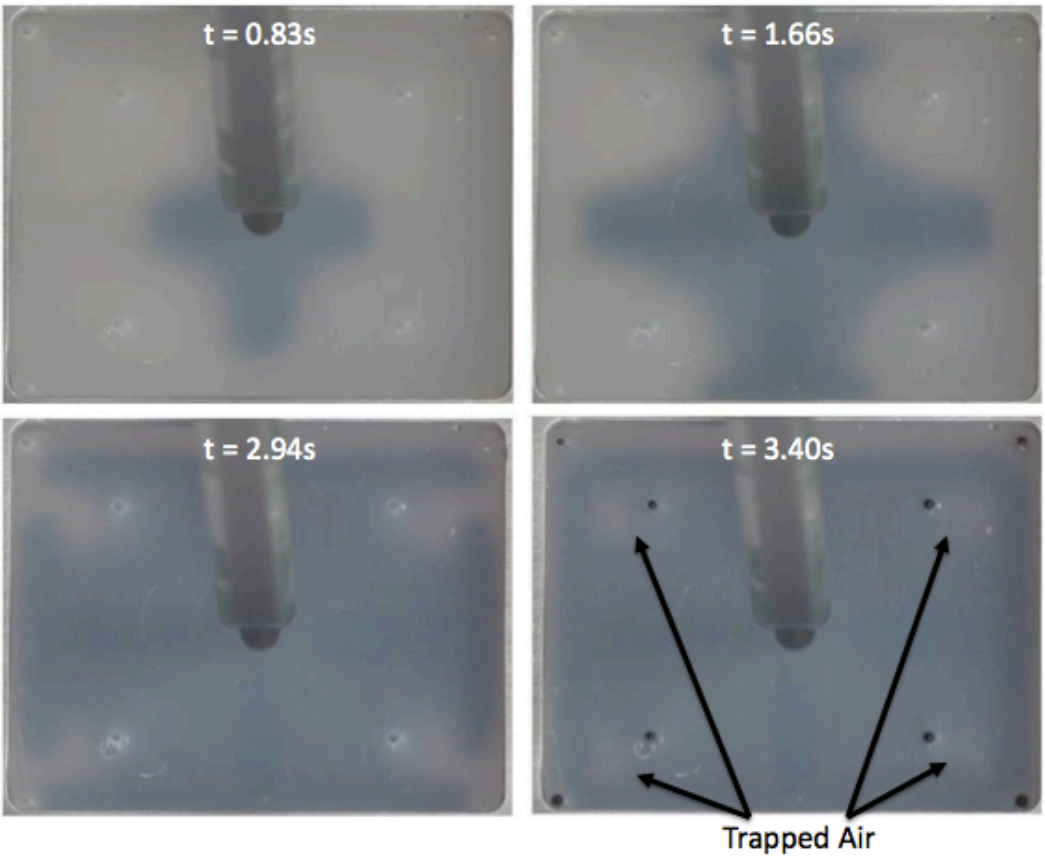

Figure 22 – Video Images – 8 Vents, Fast

Plotting the outlet concentrations versus time from the simulation for this case, a steep gradient in the outlet concentration from zero to one mol/m^3 is observed. This steep gradient in concentration coincides with the outlet surface transitioning from being filled with air (0 mol/m^3) to being filled with polymer (1 mol/m^3). That is, the flow front has reached the vents and the mold cavity has completed filling. The inflection point of this gradient, the point where the concentration gradient is at a maximum, is chosen to represent the location of the steep increase with respect to time. Figure 23 shows a plot of concentration versus time for the case with eight vents and high flow rate.

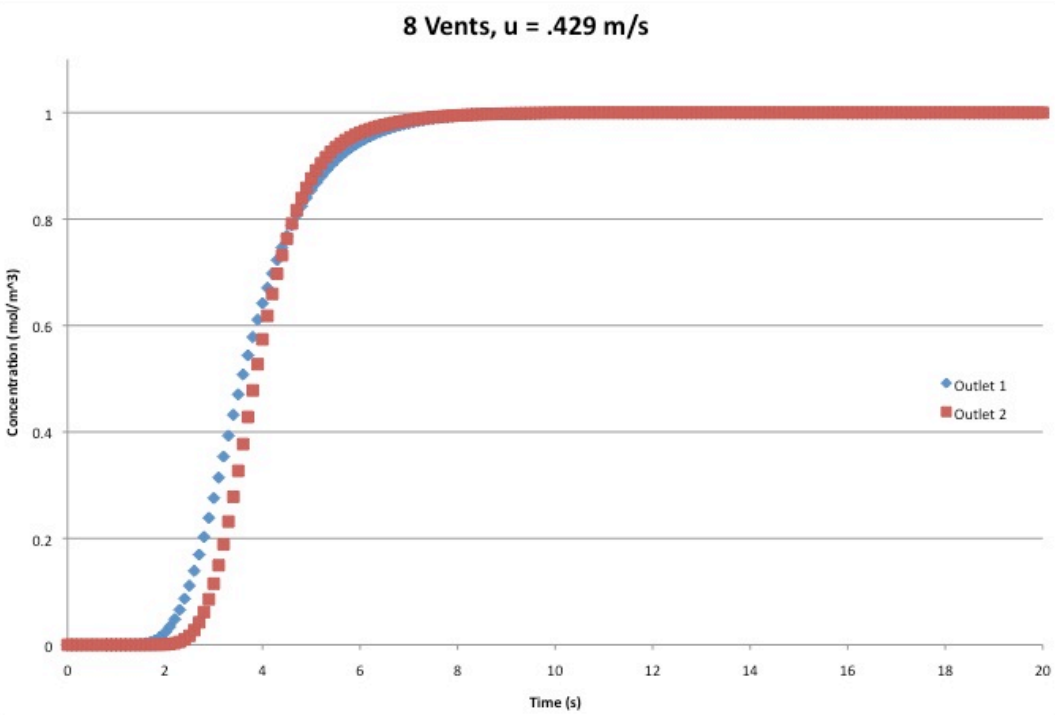

Figure 23 - Concentration vs. Time Plot, 8-Vents Fast Flow Rate Case

Concentration plots define *Outlet 1* as the outlet closest to the inlet and *Outlet 2* as the furthest. The location of this gradient can be moved with respect to time by varying the diffusion coefficient, *D*, in equation 9. By modifying the diffusion coefficient the simulation was iterated until a coefficient was found so the gradient's inflection point matched the actual time-to-fill; therefore, the inflection point represents the simulated time-to-fill. The value of the diffusion coefficient, *D*, to match the simulation to experimental data is 2.0 x 10^{-6} m^2/s. Using this coefficient value and the inlet velocities from Table 5 the different cases were simulated and the fill times from each simulation were compared to the actual fill times from the video recordings. Again, since the medium-slow flow rate and medium-fast flow rates were similar, only one case was simulated. The results of this comparison are seen in Table 6 that shows the simulated fill times are accurate with a maximum error of 8.3%.

Table 6 - Actual and Simulated Fill Times

Mold Type	12 vents	8 vents	12 vents	8 vents	12 vents	8 vents
Qualitative Velocity	Slow	Slow	Med/ Fast	Med/ Fast	Fast	Fast
Actual Time to Fill (s)	14.65	16.95	8.11	8.88	2.77	3.40
Simulated Time to Fill (s)	14.5	15.9	8.7	8.9	3.0	3.4

After determining the filling time of the simulation the concentration was plotted at all of the solution time steps. The color scale of each plot was scaled to the vent with the minimum concentration at the time when the mold is full. Using this scaling, we assumed the highest color indicator (green) represented elements that were filled, while the lowest indicator (red) represented those that were not. Intermediate concentrations (yellow) represented elements where there was uncertainty in filling, and thus were at risk for air trap defects.

The simulation solutions were compared to the experimental videos. Still frames from the combined flow and convection-diffusion simulation are shown in Figure 24. The color plots are taken on a mid-plane between the top and bottom surface of the *Array Plate*. The simulation screen captures compare well to the experimental photos in Figure 22 showing similar flow patterns at the varying time steps. Most importantly for this simulation the final time step, the filled state, shows an area of trapped air between the inner and outer vents. This trapped air volume is also visible in the experimental video captures shown in Figure 22.

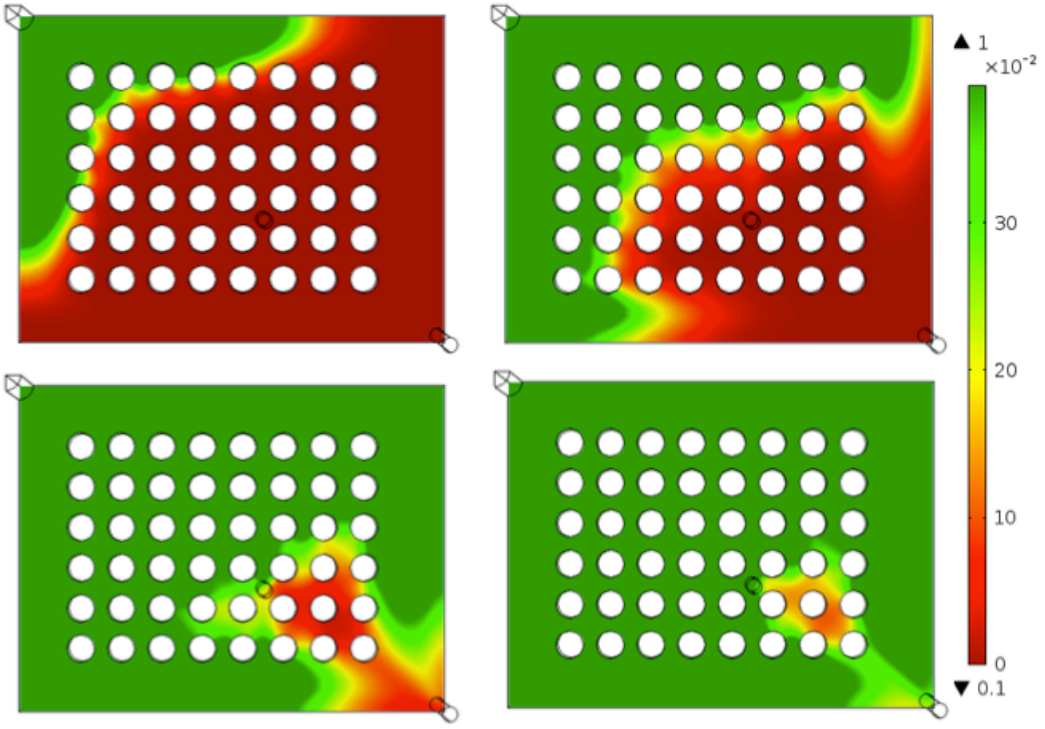

Figure 24 - Simulation Results, 8 Vents, Inlet Velocity = 0.429 m/s

Similarly, the mold case with twelve vents was simulated at a fast velocity, 0.538m/s. A few time steps of the simulation are shown in Figure 25. A flow pattern similar to the 8-vent case is observed for the 12-vent case; however, a higher concentration is observed throughout the model in the final time step. This higher concentration signifies that the mold is predicted to fill without air traps. Experimental video also shows the mold filling without air traps. Still frames from the experimental video are shown in Figure 26.

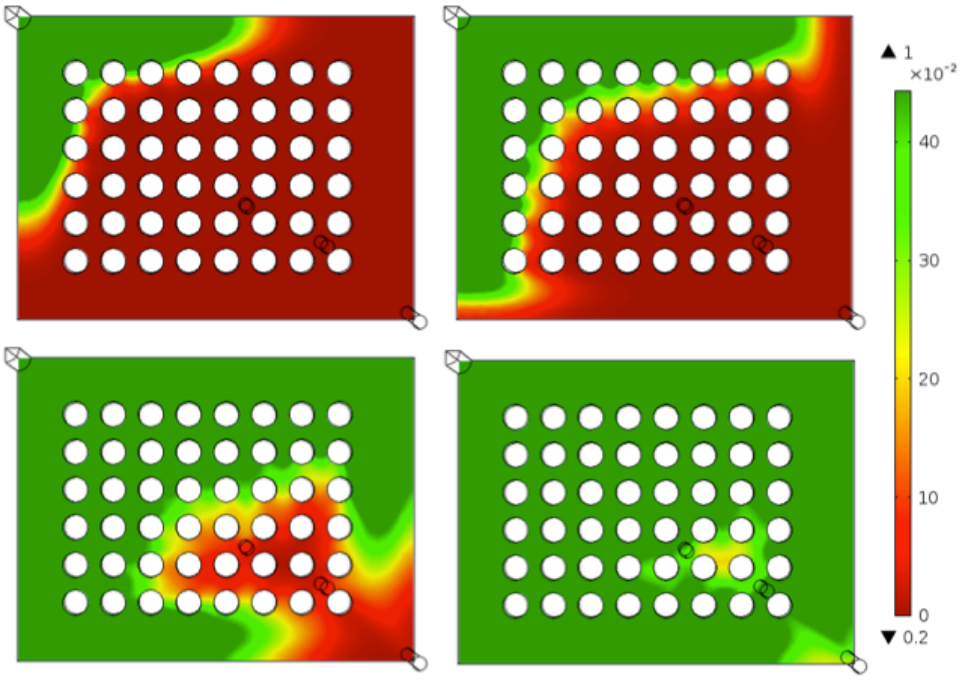

Figure 25 – Concentration Results (mol/m³), 12 Vents, Inlet Velocity = .538 m/s

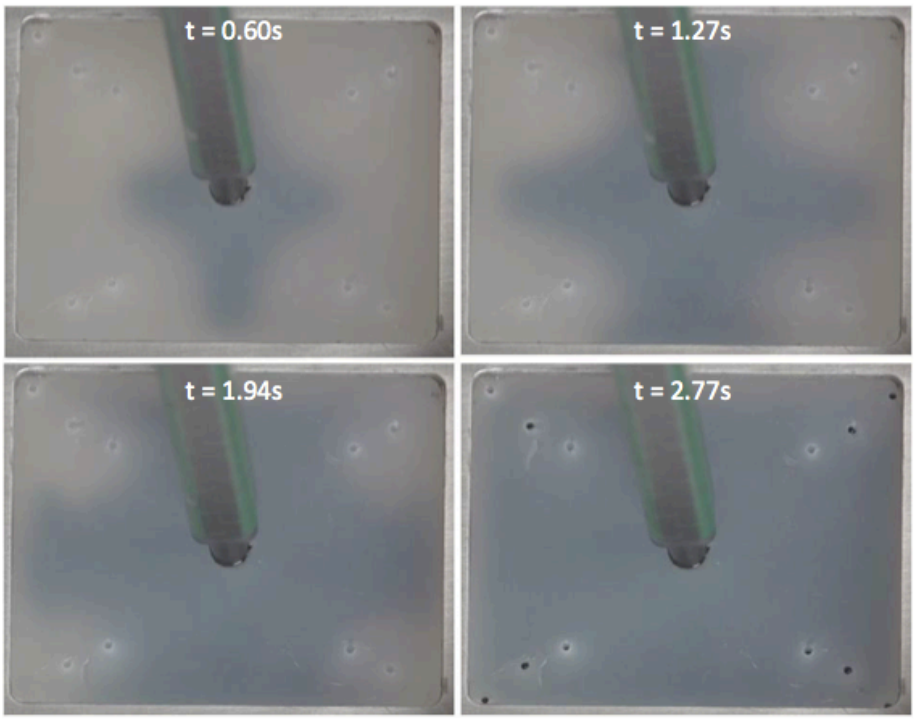

Figure 26 – Video Images – 12 Vents, Fast

The experimental and simulation data show that the *Array Plate* works well across varying velocities when twelve vents are used. At lower velocities the inflection time of the concentration varies more between each outlet. In Figure 23, the high concentration gradients at Outlet 1 and Outlet 2 occur almost simultaneously. As the inlet velocity lowers, the gradients separate with respect to time. The simulated concentration plot for the case with twelve vents at a velocity of 0.102 m/s is shown below in Figure 27. Although the gradients are separated the average time of the three inflection points, that is the simulated time-to-fill, compares well with the experimental time-to-fill as seen in Table 6.

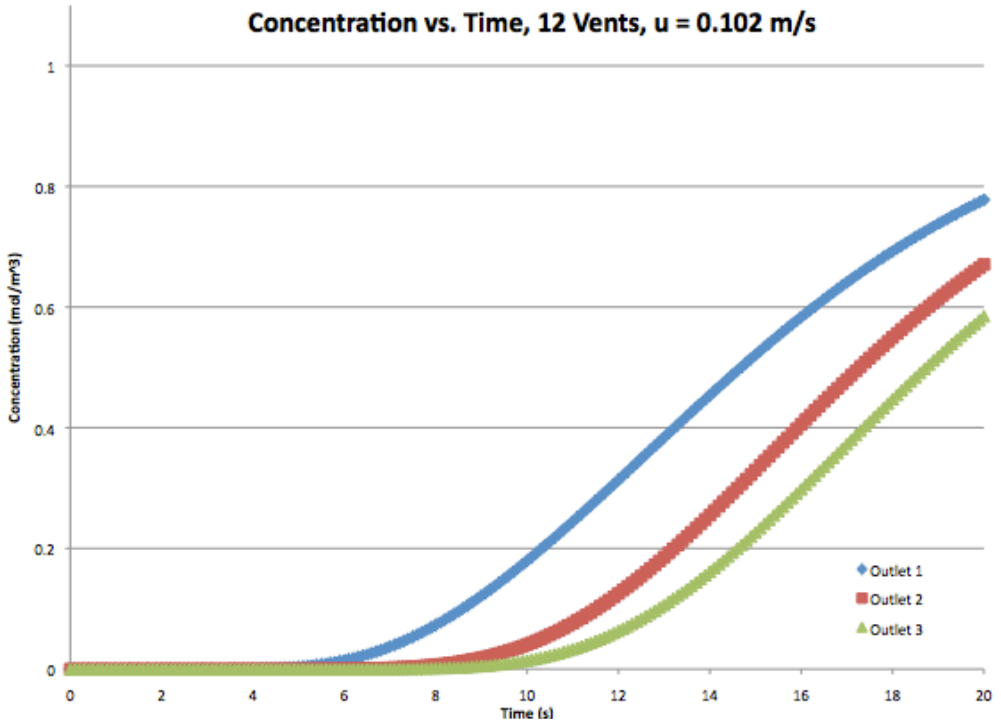

Figure 27 - Concentration vs. Time Plot, 12 Vents Slow Case

This simulation technique is shown to accurately predict the time required to fill the mold and predict where trapped volumes of air will occur in the mold cavity when the mold is filled. The technique was used to simulate the detailed geometry (including alignment features) from the experimental videos, a screen capture of the final time step for the twelve vent case using an inlet velocity of 0.538 m/s is shown in Figure 28. It can also be used to predict air traps in more detailed and varied geometries as will be shown in Section 3.4.

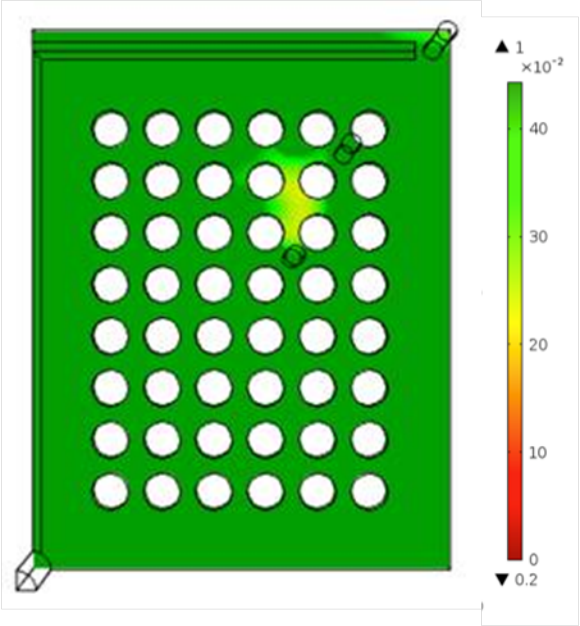

Figure 28 - Simulation Result, 12 Vents, Inlet Velocity = .538 m/s

3.4. Final Geometry Simulations and Results

After initial prototypes of the *Array Plate* and *Lateral Wall* were generated and assembled it was determined that the triangular grooves in the *Array Plate* needed to be deeper to engage better with the mating boss on the *Lateral Wall*. The depth of the alignment grooves was changed from 0.38 mm to 0.64 mm. This change was made prior to final completion of the modeling technique and the molded *Array Plates* were consistently being produced with air traps near the third outlet (furthest from the inlet) along the triangular groove. When the simulation technique was finalized, the updated *Array Plate* geometry was simulated. Figure 29 shows the simulation results indicating an air trap in the same location as those seen in the molded prototype hardware.

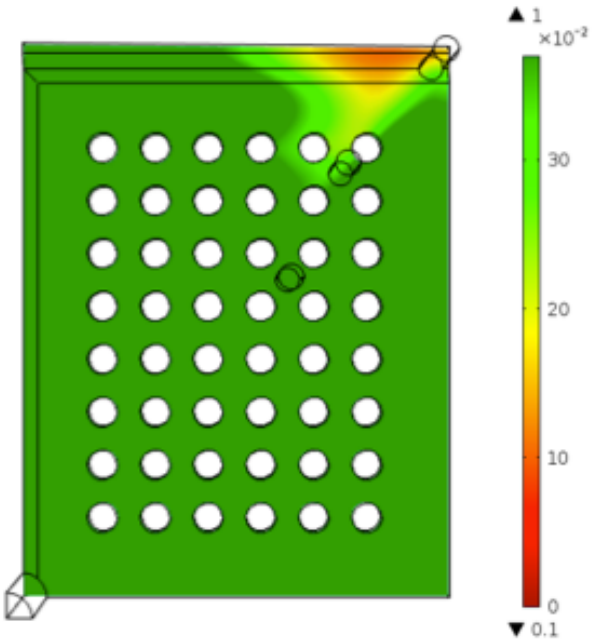

Figure 29 - Simulation Result, 12 Vents with 0.64mm Deep Alignment Grooves, Inlet Velocity = 0.538 m/s

After analyzing the results it can be seen that the reduced flow area along the length of the alignment groove causes the fluid velocity to decrease. The alignment groove acts a restriction to the fluid flow causing the flow rate to decrease. The reduced flow rate along the alignment groove allows fluid to reach the third vent (furthest from the inlet) along the edge that does not include the groove. Since the vents are filled before the mold is completely filled along the alignment groove, an air trap is left in the mold. To combat this effect a groove was added to slightly restrict flow, although there is no feature on the *Lateral Wall* to align with this feature. This feature only exists to completely fill the mold without air traps. The geometry of the additional groove is similar to the alignment groove, only shallower. A few different

depths of the geometry were analyzed and the analysis shows that a depth of 0.38 mm would result in the best mold filling across all injection velocities. Concentration plots for the varying injection velocities are shown at their fill time in Figure 30 for the geometry with additional, flow-restriction grooves. The value *u* in Figure 30 indicates the inlet velocity and the value *t* indicates the simulation time at which the screen capture was taken, in this case the fill time.

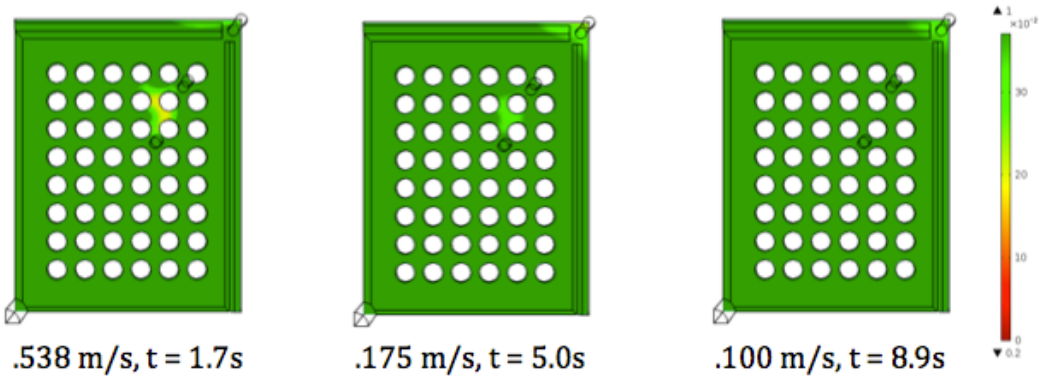

Figure 30 - Concentration Plots, Array Plate with Additional Groove

As these concentration plots show, the mold for this geometry is expected to fill properly across all inlet velocities. This is the final design geometry for the *Array Plate* and initial prototypes of this geometry do fill completely generating useable parts for the cartridge assembly.

The simulation technique was also expanded to include the *Lateral Wall*. The analytical model for this part is a half-symmetry model. The plane of symmetry is highlighted in the meshed model shown in Figure 31. For this

geometry, there are four vents; two are included in the analysis, at the furthest point from the inlet. The inlet and outlets are indicated in Figure 31.

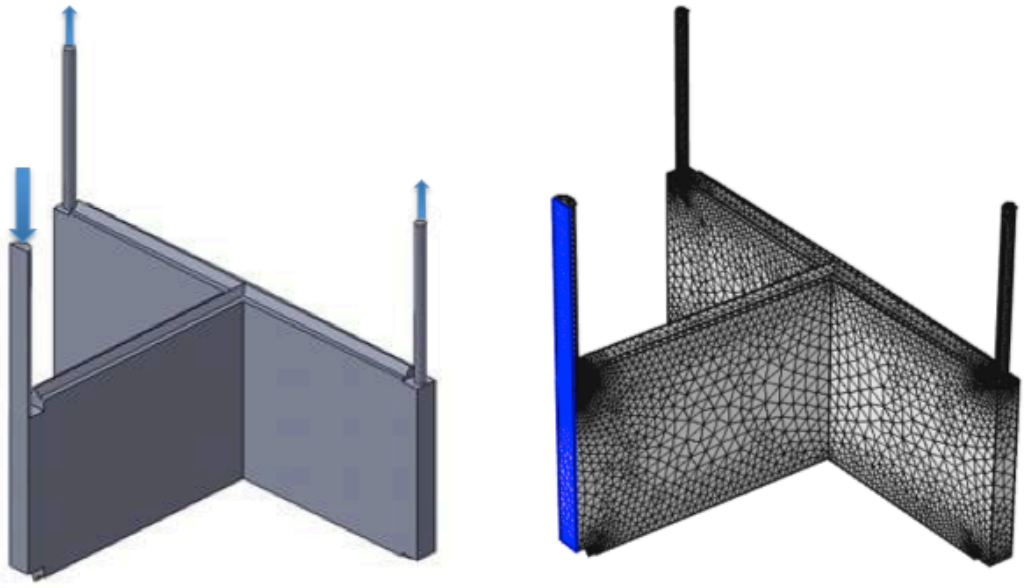

Figure 31 - Lateral Wall CAD Model (l) and Analytical Model (r)

Initial prototypes for this part entirely filled the cavity consistently; however, when the alignment feature was adjusted, air traps consistently formed in the area circled in Figure 32. Initially it was hypothesized that air traps were formed due to the sharp corner where the alignment feature transitions to the vent and air in the mold would get caught in the sharp feature with no way to exit as the fluid continues to flow underneath it.

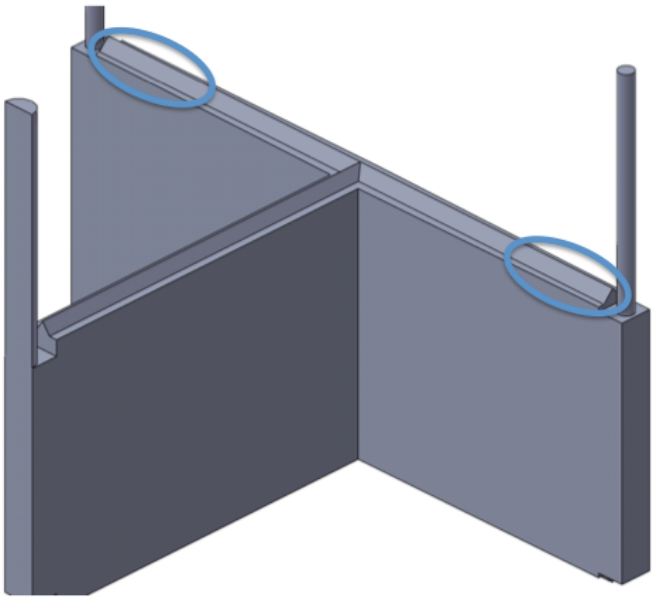

Figure 32 - Lateral Wall, Alignment Boss Detail

A parametric sweep of inlet velocity was performed on the *Lateral Wall* geometry; results are shown in Figure 33. Analysis aided us in understanding where the air trap occurs as it shows that they form in the bottom corner of the cavity underneath the vent, not in the areas circled in Figure 32. This led us to hypothesize that after a short time the trapped air will float toward the vent; however, it does not consistently escape which we suspect to be caused by the surface tension of the fluid. Using this information from the simulation, it was shown by generating prototypes that we can wait after the initial injection for the trapped air to float towards the vent and then perform a second injection to push the bubble out. As the simulations show, a slower injection velocity leads to a smaller volume of trapped air and therefore a higher probability that the trapped air volume will float to the vent location. This method of injecting has been proven successful after initial prototypes

determined the correct amount of time to wait prior to introducing the second injection. Alternatively, the injection rate could be slowed significantly so that no trapped air volume exists; however, the flow rate for this approach has not been determined and the preferred method is to do a second injection as it has already been proven to produce consistent lateral wall parts.

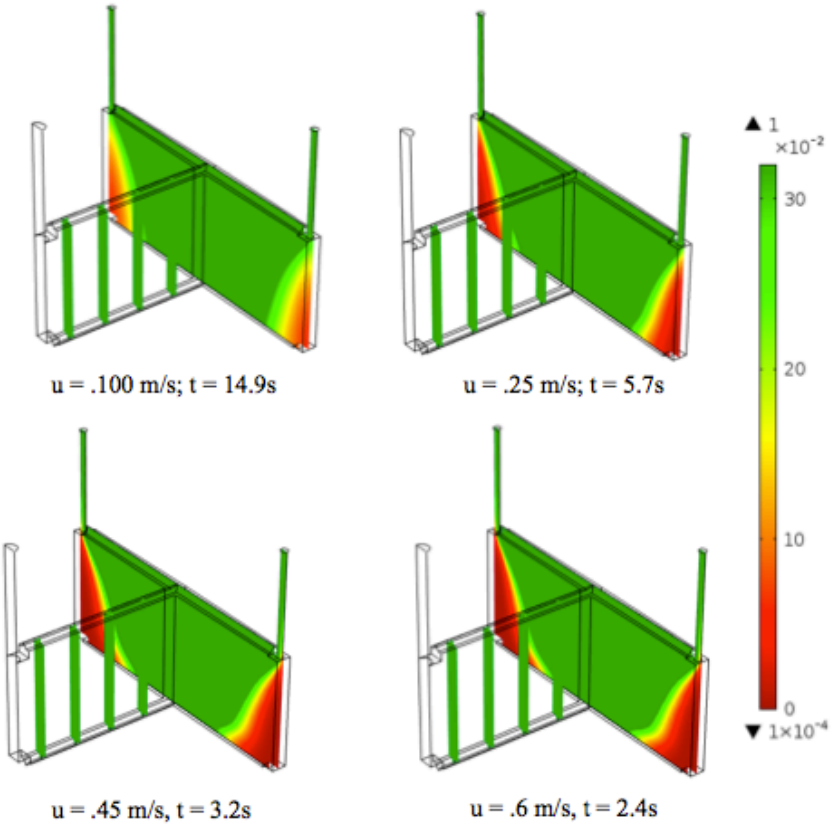

Figure 33 - Concentration Plots, Lateral Wall

3.4.1. Péclet Number Analysis

With the high value of the diffusion coefficient used in these simulations, the diffusion model is proven to have an effect on the flow front in the areas of the model where the flow is restrictive. Along the edges of the models, the flow is driven by convection; however, in the area of the holes, the simulated transport is driven by diffusion. This is proven by evaluating the Péclet Number (Pe) for the *Array Plate* model. The Péclet Number is a dimensionless value that compares convective transport to diffusive transport by the equation:

$$Pe = \frac{Lu}{D} \qquad [14]$$

where L is the characteristic length; u is the magnitude of fluid velocity; and D is the diffusion coefficient. The Péclet number values were calculated for the final array plate geometry that coincides with the results displayed in Figure 30 as well as Figure 52 through Figure 57 in Appendix B. For this geometry, the maximum Péclet number occurs at the inlet using the inlet diameter as the characteristic length; the minimum occurs between holes in the area of the vents where minimum velocity occurs (see Appendix B) using the minimum distance between holes as characteristic length; and the average value was calculated using a volumetric average velocity and the inlet diameter as the characteristic length.

Table 7 - Péclet Number Analysis of the Array Plate

Inlet Condition	Minimum Pe	Maximum Pe	Average Pe
u_{in} = 0.538 m/s	0.2	546.6	31.3
u_{in} = 0.175 m/s	0.07	177.8	10.2
u_{in} = 0.100 m/s	0.03	101.6	5.8

Using these results we can see that the average and maximum Péclet numbers indicate dynamics that are convection dominated (Péclet number 5.8 to 546). However, in regions where the flow velocity is very low Péclet numbers on the range of 0.03 to 0.2 were found, indicating the importance of diffusive transport in these regions. These regions only take up a small portion of the overall model but are locations that would take a prolonged time to fill if the simulations only accounted for convection leading to incorrect interpretation of remnant air traps. While in actuality air is replaced by polymer during the filling process in a time-dependent fashion, our steady flow simulations did not take the liquid-gas interface into account but instead used a diffusion parameter to allow experimental matching to real-world phenomena. As the simulation relies more on diffusion, more care will need to be taken when interpreting model results as we use diffusion as a smoothing parameter rather than as a representation of the true underlying physics.

3.5. Discussion and Next Steps

The solution obtained for the diffusion coefficient used in these simulations was very high; however, these simulations do not find solutions for the flow front over time by solving the true underlying physics. Rather, the species transport model is a simplified method for determining the approximate location of the polymer flow front over time based on comparison to experiments. By comparing the simulation results to experimental data we have found this simulation technique to be reasonably accurate for the micro-fluidic cartridge parts. Future work pertaining to this technique must be performed to assess its ability to be generalized and determine the criteria when it can accurately predict mold filling.

Péclet Number This chapter has discussed the minimum, maximum and average Péclet number for the *Array Plate* part in its final geometry. We suspect that the effectiveness of this technique will depend on the Péclet number, that is, the convective dependence of the total species transport versus the diffusive dependence. Areas of the transport model with a low Péclet number are more heavily affected by the diffusion coefficient as in the resistive regions between holes in the array plate. It is worth noting that the equations governing flow in a resistive, porous media (Darcy's Law) are analogous to the governing equations of diffusion. We suspect that this problem of flow through a cavity with numerous, regularly-spaced, resistive elements begins to approximate flow in porous media and helps to explain

why modeling using diffusive properties may provide good match with experimentation. However, it also cautions that parts with irregularly spaced resistive elements may not be modeled well using a single diffusion parameter.

Part Size and Orientation The simulations were done using the assumption that the body force, gravity, is negligible. This assumption was acceptable for these simulations of steady flow in a liquid-filled cavity. With air-filled chambers that are replaced by fluid, buoyancy and gravity are present but likely remain a second order effect in our process. Indeed, in filling of the lateral wall chambers, air bubbles remained at the bottom of the mold for the duration of filling and required a 30 second waiting period after the initial injection to allow air to float and be vented, greater than the ~5 second injection time used in simulations. This assumption, although valid for simulations of cartridge parts, will need to be reconsidered for varying mold designs.

3.6. Summary

This chapter discusses the development of an analytical tool to use for generating part geometry that is robust to the variability involved of a user-controlled injection process for reaction injection molding. It discusses the use of *COMSOL Multiphysics* as an analytical tool as well as the use of video to provide necessary model inputs for the simulations. It also discusses

analytical results and how they were used to inform the design and production of micro-fluidic cartridge parts.

Using a fluid flow analysis coupled with a convection-diffusion model allows us to approximate how a two-part polyurethane fluid will fill a mold cavity. From the analysis we can determine when a mold will fill and where air traps may form that would lead to the incomplete filling of parts. Since the injection portion of the reaction injection molding is user-controlled in this case, the analysis can be used for simulating multiple injection rates to ensure the part geometry is robust to the user input.

This method of simulating the mold filling provided us with the insight necessary to redesign the *array plate* parts so that they would fill without voids across a variety of injection flow rates. Array plate filling times from 3 to 16 seconds are able to reproducibly fill the designed mold cavity. It also provided insight into the injection of the *lateral wall* where rapid filling in 3 seconds can be performed although it is critical to have a 30 second waiting period prior to a second, brief injection to purge remaining air traps. Prototype molds of both parts have been made and shown to generate parts free of voids.

4. Conclusions

4.1. Thesis Contributions

This thesis directly addresses a challenge facing researchers that have trouble determining which process to use when translating new medical devices from the research stage to meet the needs for clinical trials. It goes through a down-selection process to determine the best method for manufacturing rigid polymer parts for a micro-fluidic cartridge used to study blood clotting. It also describes a simplified technique for analyzing the part designs to ensure they are robust to user-controlled fluid injection rates as well as providing feedback to ensure proper mold design.

Due to its low risk, low cost, and its ability to quickly generate prototype parts, reaction injection molding was the process selected for creating the micro-fluidic cartridge parts. The molding process was modified for use in a laboratory setting without the need for industrial equipment to meet the required quantity of parts (100-1000) needed for clinical trials. The process relies on 3D printed mold masters to generate silicone molds. Molds are then hand-injected with a two-part liquid polyurethane that cures in the mold to create rigid plastic parts accurately with tolerances similar to those of the current 3D printed parts and cost-effectively (less than $4 per cartridge).

The work done in this thesis aided in contributing micro-fluidic cartridge parts to the Clinical Research Center at MIT permitting continuation of scientific efforts that will lead to validation, publications, and development of a clinical diagnostic tool. The reaction injection molding technique developed by this thesis also allows CRC to create parts in their laboratory and also developed a technique that may be useful at Draper Laboratory.

Beyond development of manufacturing method and part production, an efficient computational technique for simulating mold filling was developed using a fluid flow analysis coupled with a convection-diffusion model. This approach allows the user to determine when the mold is filled as well as determine where trapped volumes of air may yield poor quality parts. Model geometry and/or mold filling technique can then be adjusted according to the simulation results to ensure the part fills properly across a variety of injection flow rates. Final part geometries were modified based on the simulation results the validity of the simulation approach was evaluated by generating prototype parts using this geometry. Success was achieved as parts were molded without any voids caused by trapped volumes of air.

We suspect that this method for simulating mold filling has limitations although the potential constraints were not studied for this thesis. We suspect that the size of parts analyzed and the Peclet number values for the combined convective and diffusive transport may define the restrictions of this analytical technique and inform the basis for future study. We anticipate

that definitive criteria for when this technique can be used successfully can be developed and will lead to additional conference proceedings and/or publications.

4.2. Impact

The use of 3D printed mold masters in the reaction injection molding process described in this thesis means that geometries can be readily modified, making the process relevant for other geometries. Although this thesis concentrates on a specific microfluidic cartridge application, many applications require low to mid-scale quantities of small plastic parts where the overhead cost of injection molding is not justified and the cost of 3D printed parts becomes prohibitive. This thesis describes how the reaction injection molding process fills a gap in meso-scale manufacturing where other manufacturing methods fall short. Moreover, we demonstrate how modeling and simulation can be leveraged to improve the robustness and reliability of a low-cost, benchtop manufacturing process ideal for medical device translation.

A Appendix A: Experimental Video Results

Table 8 - Experimental Video Results

Mold Type	12 vents	8 vents	12 vents	8 vents	12 vents	8 vents	12 vents	8 vents
Qualitative Velocity	Slow	Slow	Med/ Slow	Med/ Slow	Med/ Fast	Med/ Fast	Fast	Fast
Mold Volume (mL)	2.949	2.890	2.949	2.890	2.949	2.890	2.949	2.890
Start (frame #)	101	80	186	145	133	138	199	123
Start (time, s)	3.37	2.67	6.21	4.84	4.44	4.60	6.64	4.04
Finish (frame #)	540	588	440	435	376	404	282	223
Finish (time, s)	18.02	19.62	14.68	14.51	12.55	13.48	9.41	7.44
Time to Fill (s)	14.65	16.95	8.48	9.68	8.11	8.88	2.77	3.40
Flow Rate (mL/s)	0.20	0.17	0.35	0.30	0.36	0.33	1.07	0.85
Velocity (m/s)	.102	.086	.176	.151	.183	.164	.538	.429

B Appendix B: Finite Element Analysis Results

Below are the results from the finite element analyses using the combined flow and diffusion models. The diffusion coefficient used for these results is $2x10^{-6}$ m^2/s obtained from Chapter 3.3. The viscosity and density of the fluid are defined in Chapter 3.2.3. Each set of results shows the plot of outlet concentration versus time that was used to determine the simulated fill time. The results also show the steady-state velocity and pressure results as well as the concentration at the time-step when the cavity is filled.

The results in Figure 35 through Figure 40 are for the simplified 8-vent *array plate* geometry that does not include the triangular alignment groove, shown in Figure 34.

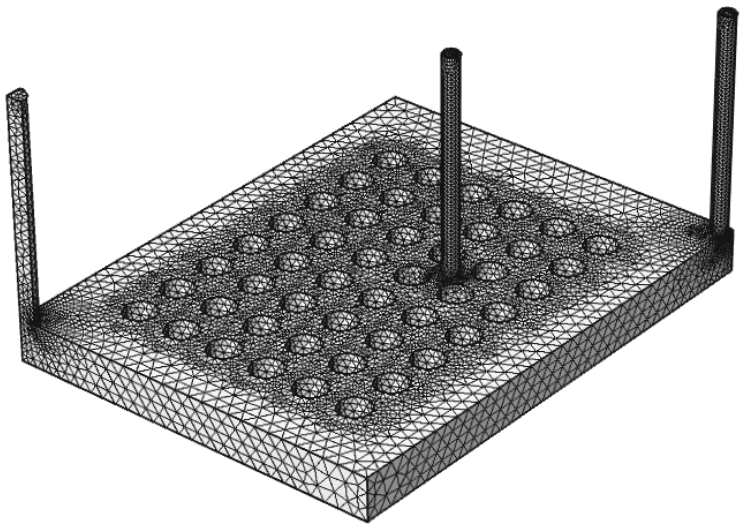

Figure 34 - Finite Element Model, Simplified 8 Vents

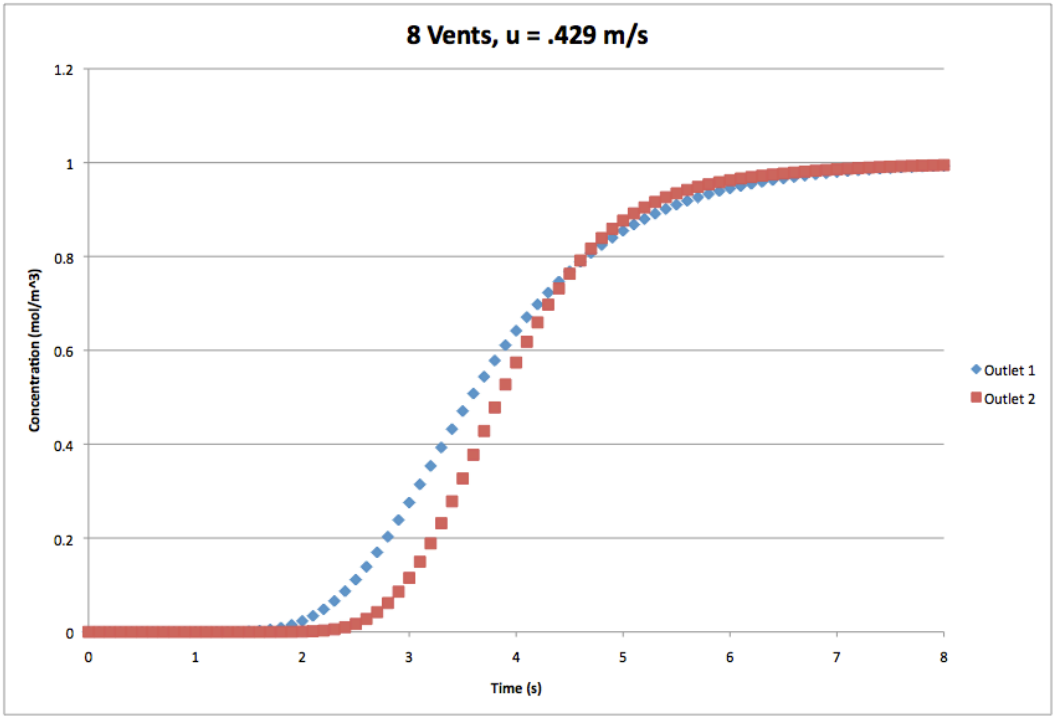

Figure 35 - Concentration vs. Time, Simplified 8 Vents, u = 0.429 m/s

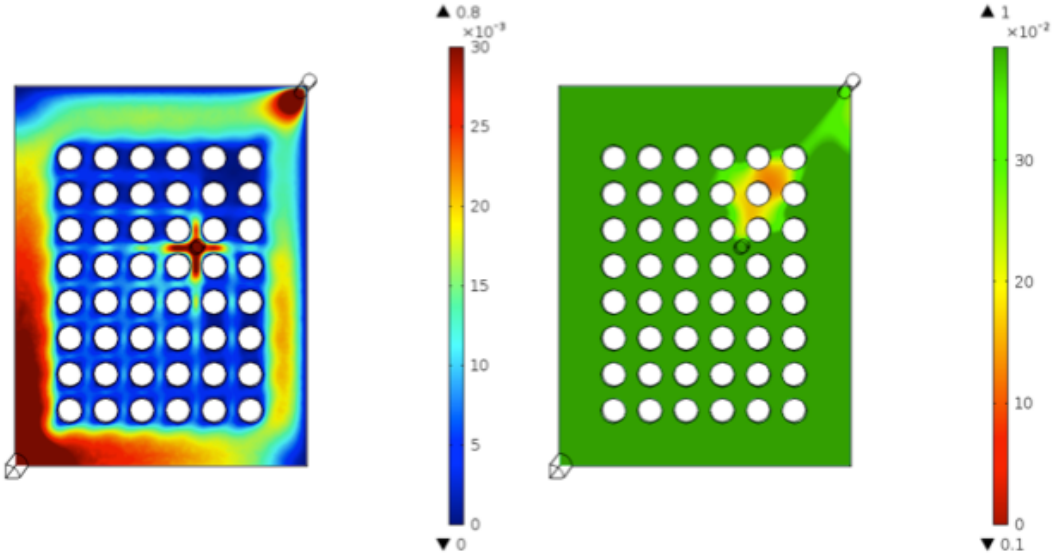

Figure 36 - Steady State Velocity and Concentration at Fill FEA Results, Simplified 8 Vents; u = 0.429 m/s, t_{fill} = 3.4 s

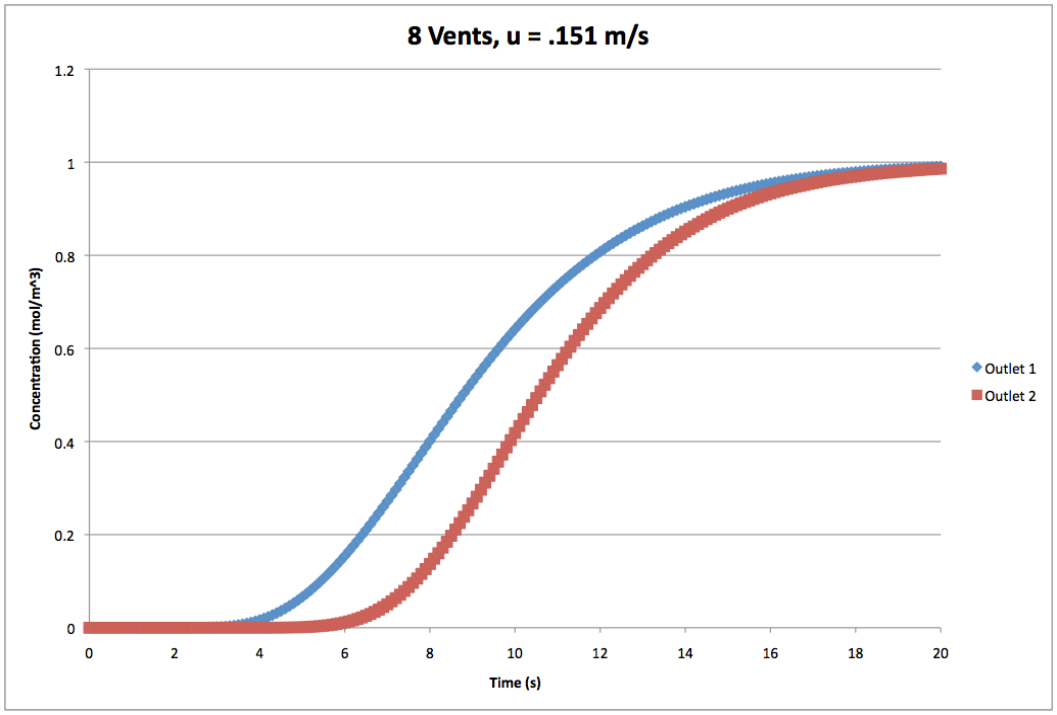

Figure 37 - Concentration vs. Time, Simplified 8 Vents, u = 0.151 m/s

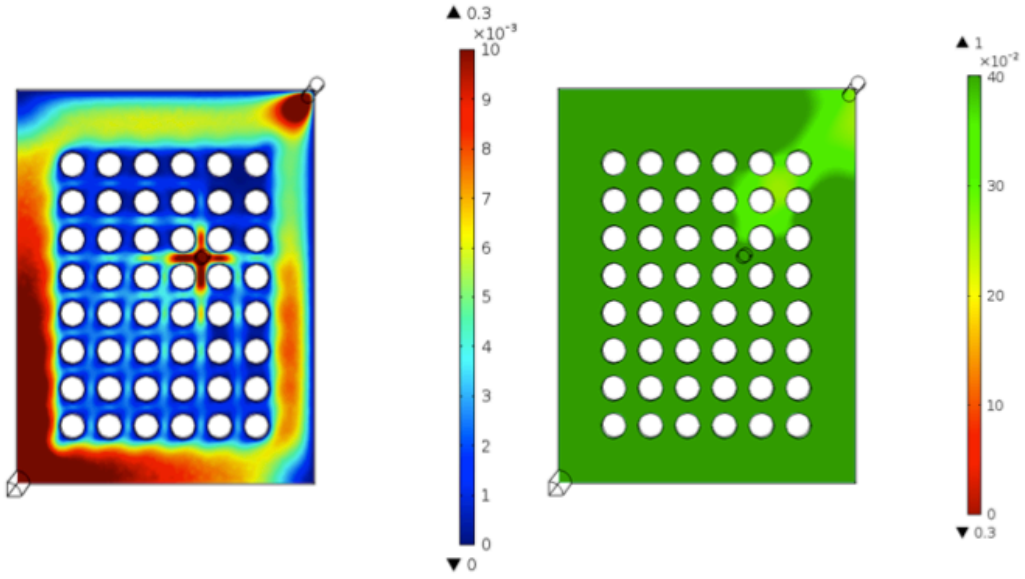

Figure 38 - Steady State Velocity and Concentration at Fill FEA Results, Simplified 8 Vents; u = 0.151 m/s, t_{fill} = 8.9 s

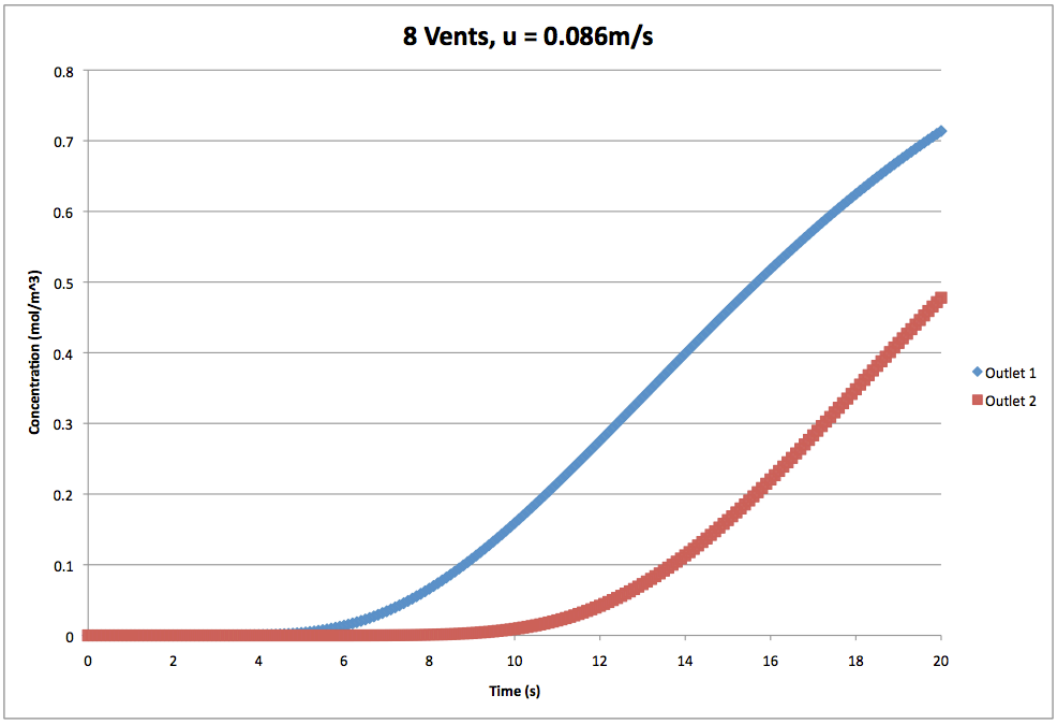

Figure 39 - Concentration vs. Time, Simplified 8 vents, u = 0.086 m/s

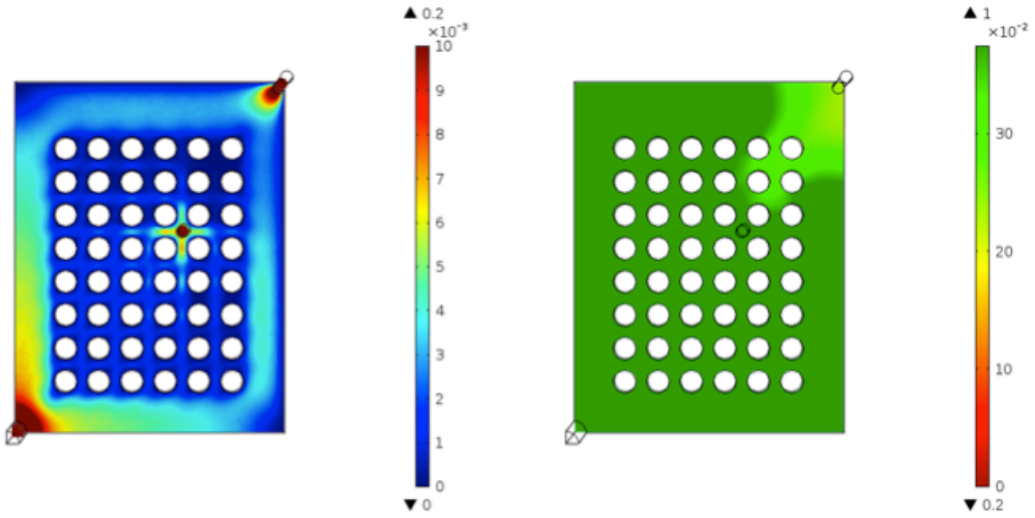

Figure 40 - Steady State Velocity and Concentration at Fill FEA Results,

Simplified 8 Vents; u = 0.086 m/s, t_{fill} = 15.9 s

The results in Figure 42 through Figure 47 are for the simplified 12-vent *array plate* geometry that does not include the triangular alignment groove, shown in Figure 41.

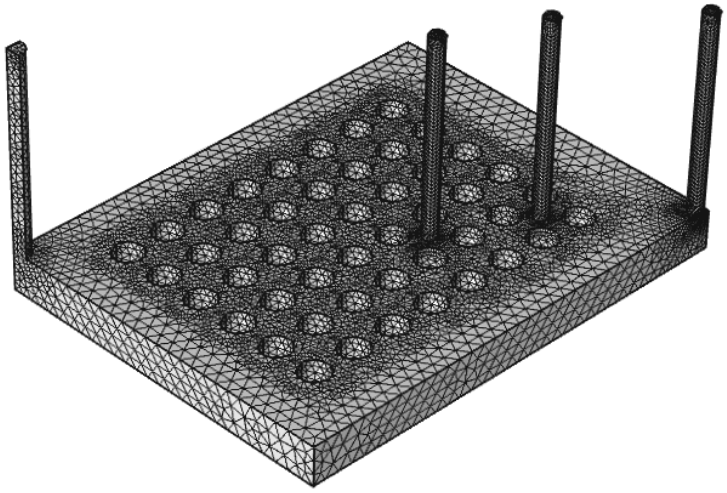

Figure 41 - Finite Element Model, Simplified 12 Vents

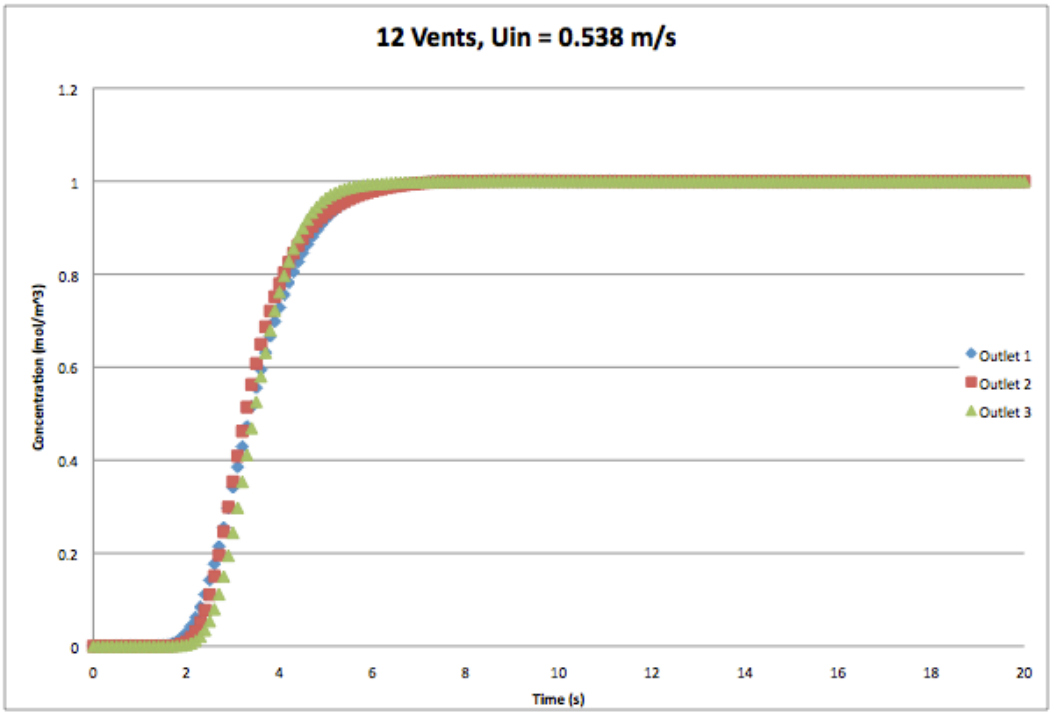

Figure 42 - Concentration vs. Time, Simplified 12 vents, u = 0.538 m/s

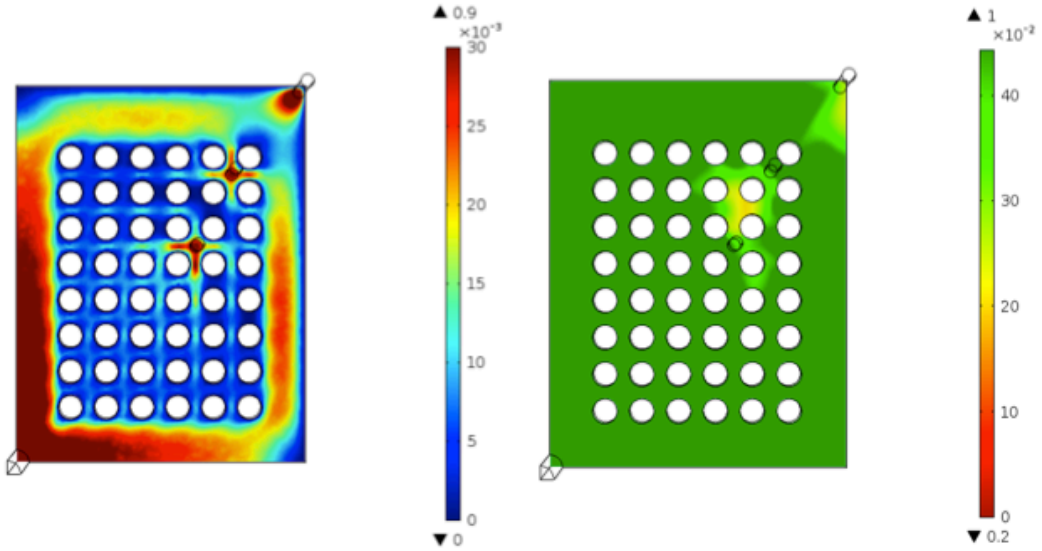

Figure 43 - Steady State Velocity and Concentration at Fill FEA Results, Simplified 12 Vents; u = 0.538 m/s, t_{fill} = 3.0 s

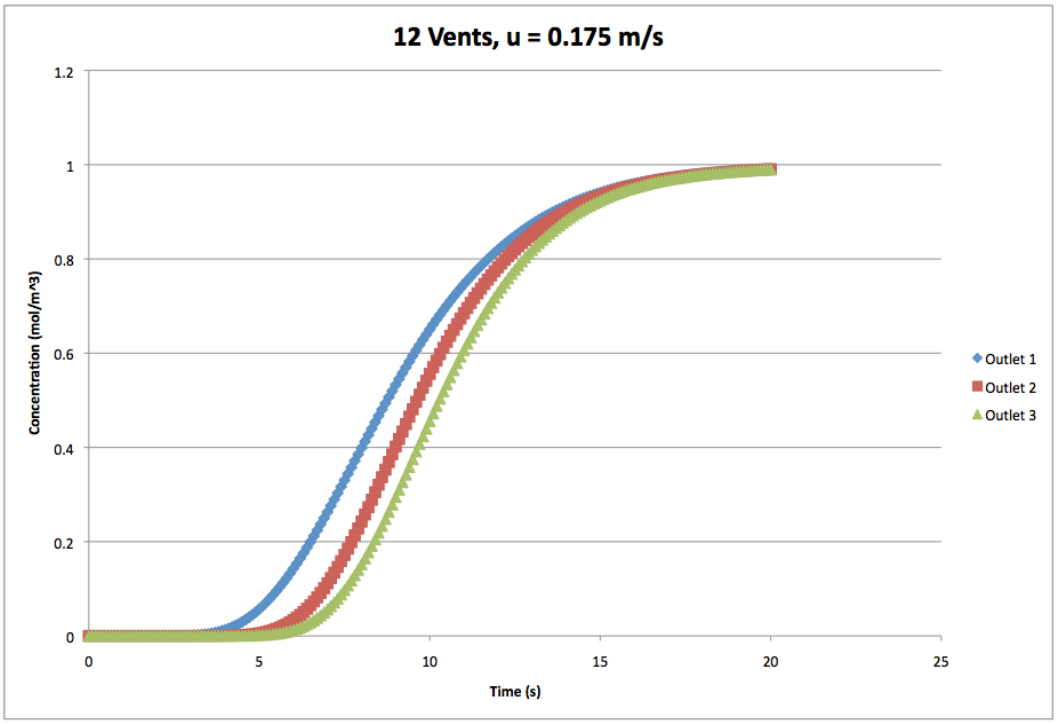

Figure 44 - Concentration vs. Time, Simplified 12 vents, u = 0.175 m/s

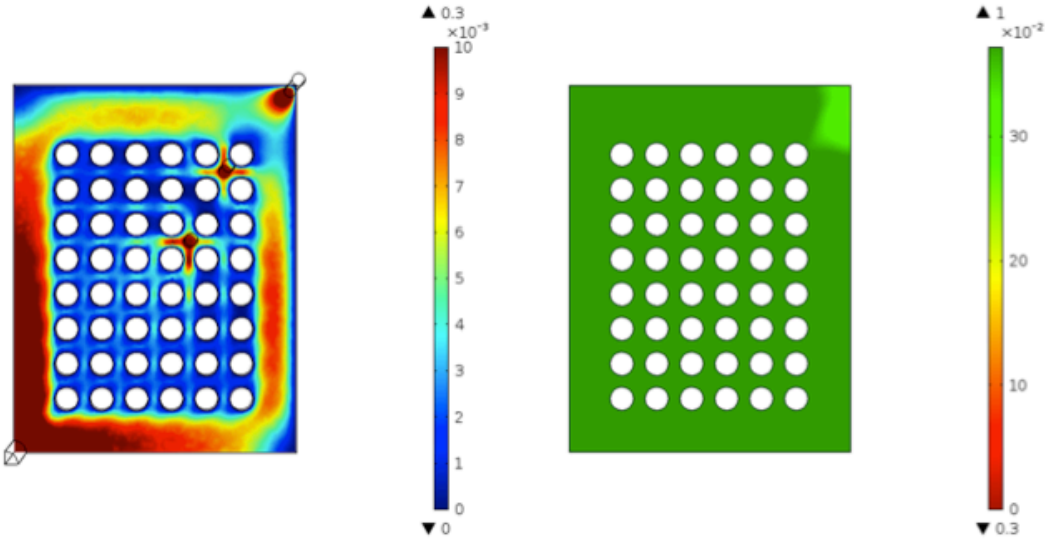

Figure 45 - Steady State Velocity and Concentration at Fill FEA Results, Simplified 12 Vents; u = 0.175 m/s, t_{fill} = 8.7 s

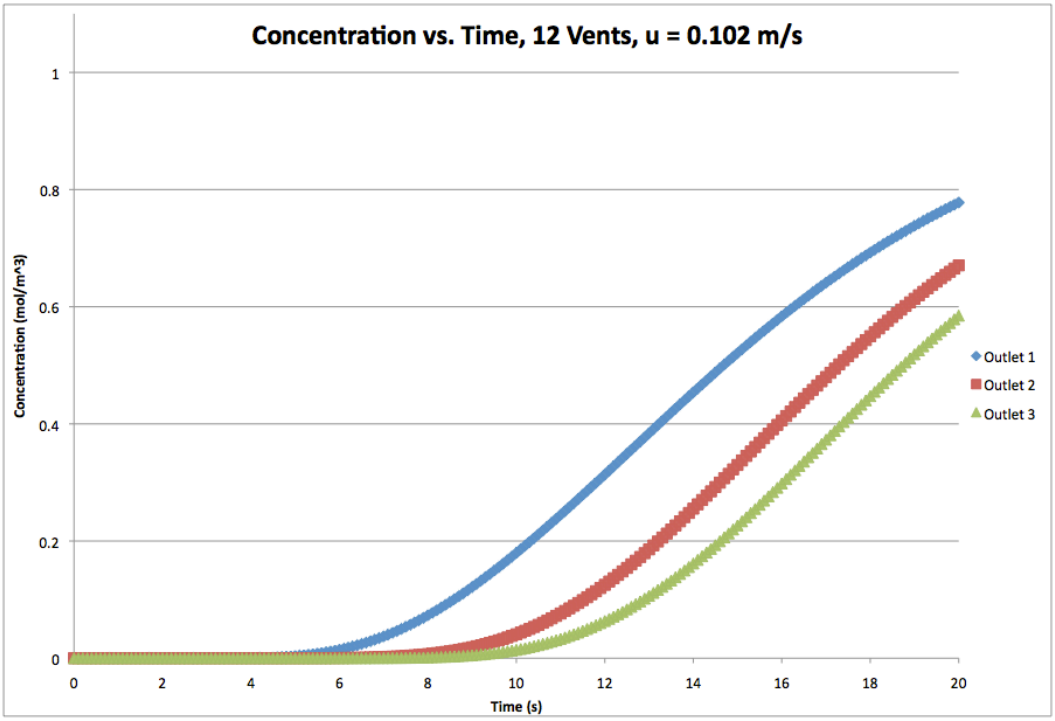

Figure 46 - Concentration vs. Time, Simplified 12 vents, u = 0.102 m/s

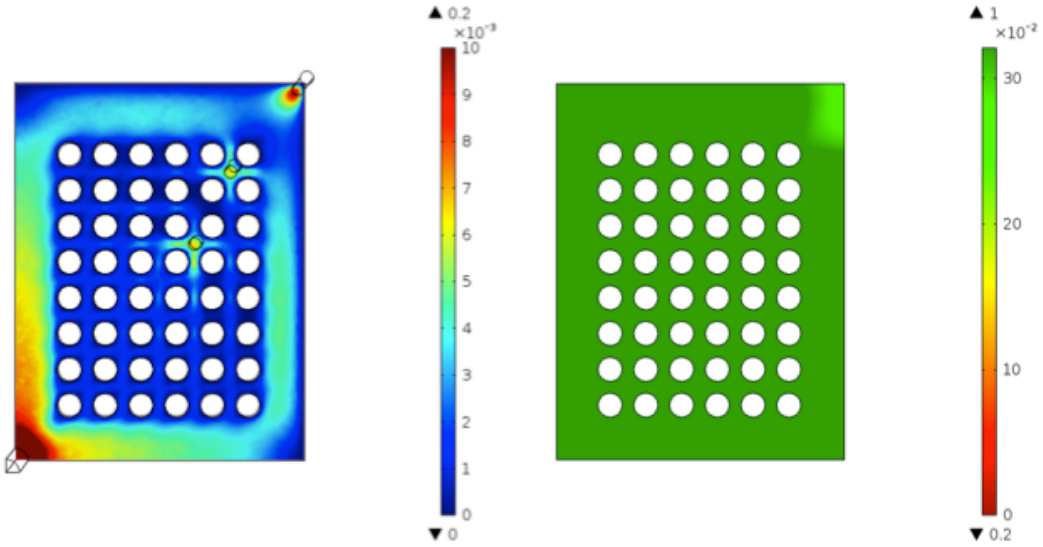

Figure 47 - Steady State Velocity and Concentration at Fill FEA Results, Simplified 12 Vents; u = 0.102 m/s, t_{fill} = 14.5 s

The results in Figure 49 and Figure 50 are for *array plate* geometry with 12 vents and a 0.635mm deep alignment groove as shown in Figure 48.

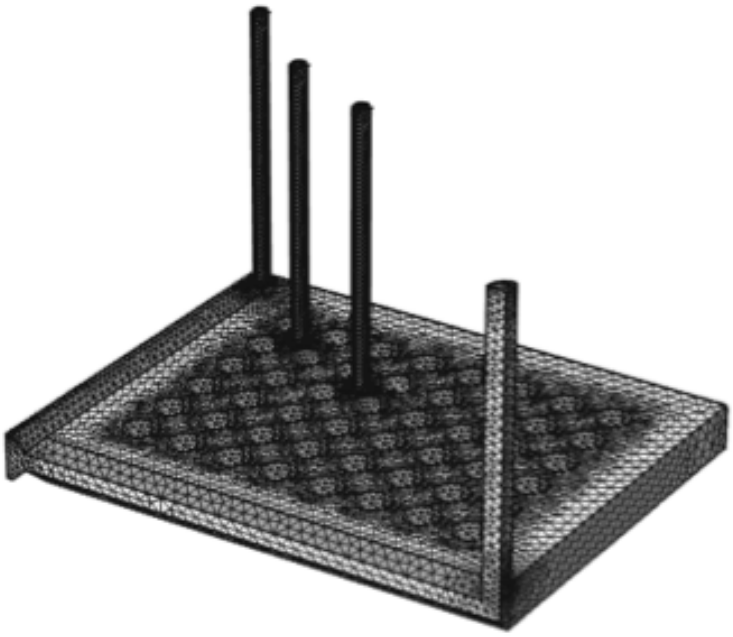

Figure 48 – Finite Element Model, 12 Vents with 0.635 mm Deep Alignment Grooves

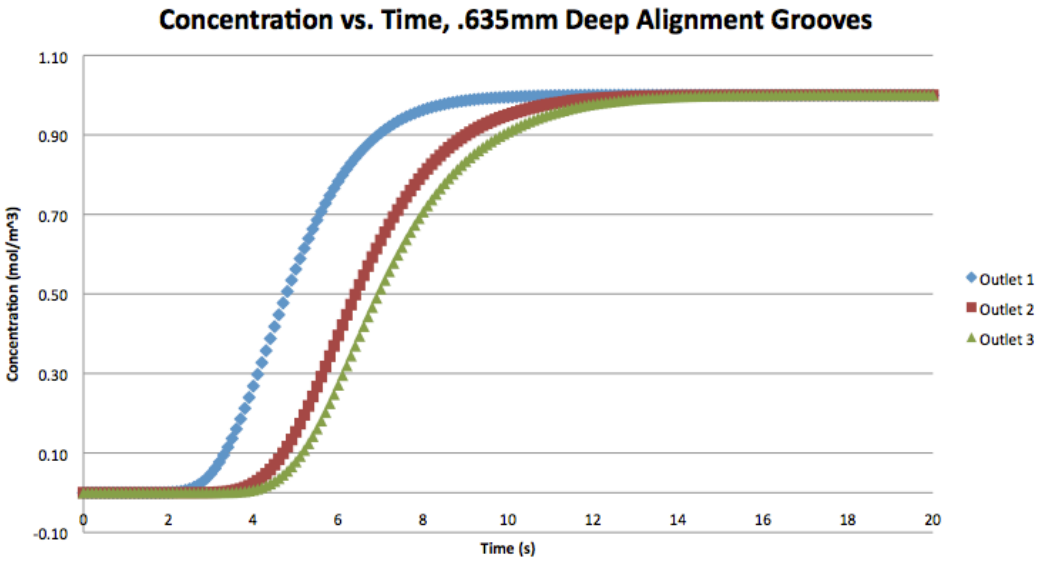

Figure 49 – Concentration vs. Time, 0.635mm Deep Alignment Groove, u = 0.175 m/s

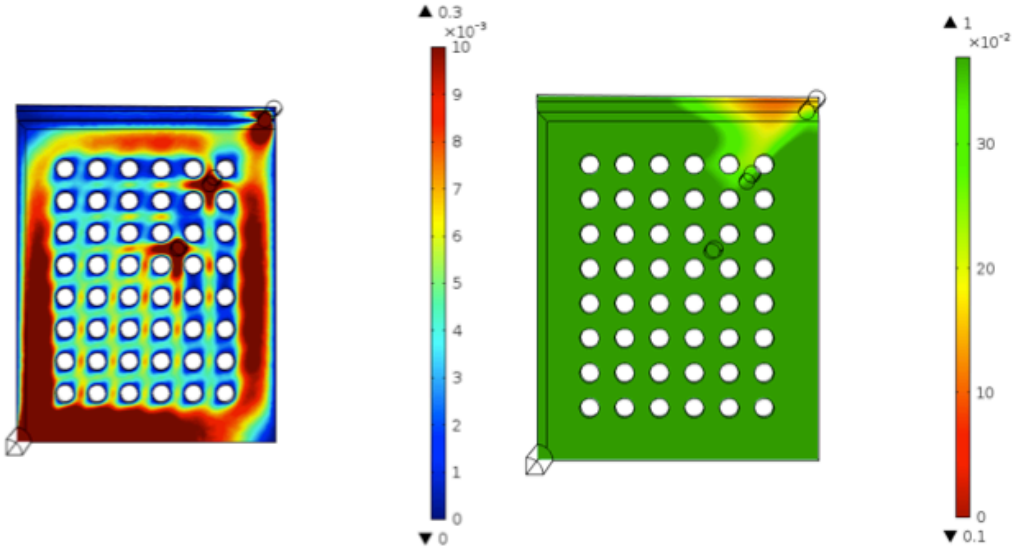

Figure 50 - Steady State Velocity and Concentration at Fill FEA Results, 0.635mm Deep Alignment Groove; u = 0.175 m/s, t_{fill} = 5.6 s

The results in Figure 52 through Figure 57 are for *array plate* geometry with 12 vents, a 0.635mm deep alignment groove and an additional 0.375mm groove used to balance flow from the inlet. The finite element model for this case is shown in Figure 51.

Figure 51 - Finite Element Model, 12 Vents with 0.635 mm Deep Alignment Groove and Additional Groove

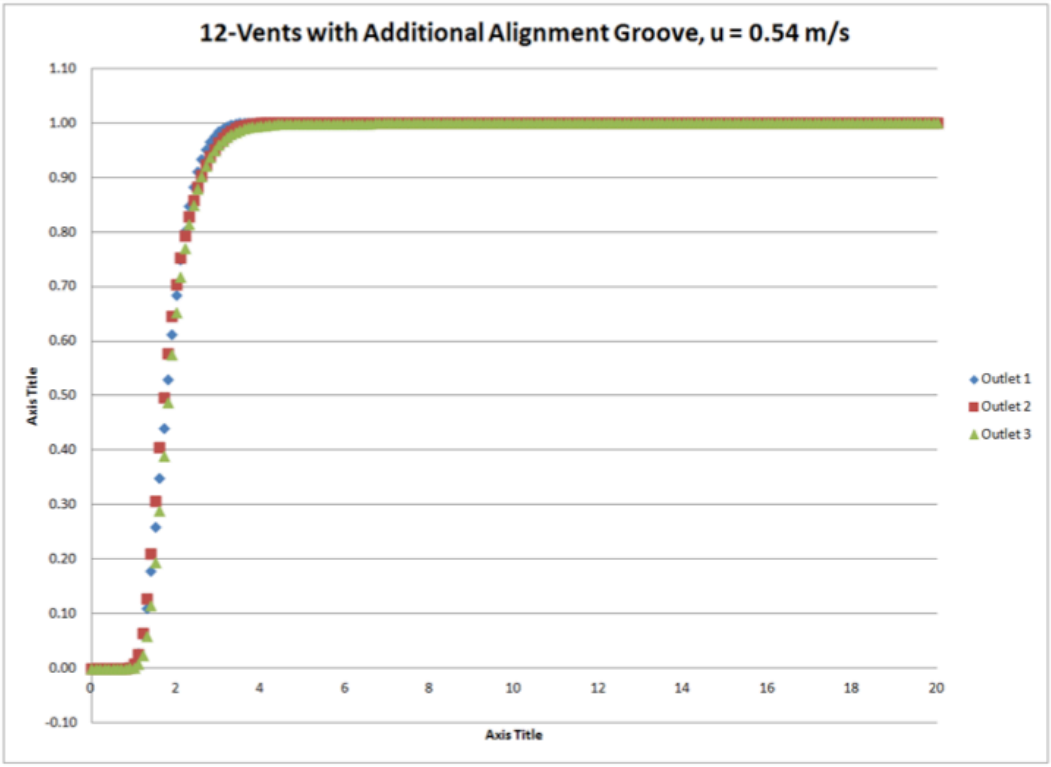

Figure 52 - Concentration vs. Time, 0.635mm Deep Alignment Groove with Additional Groove, u = 0.538 m/s

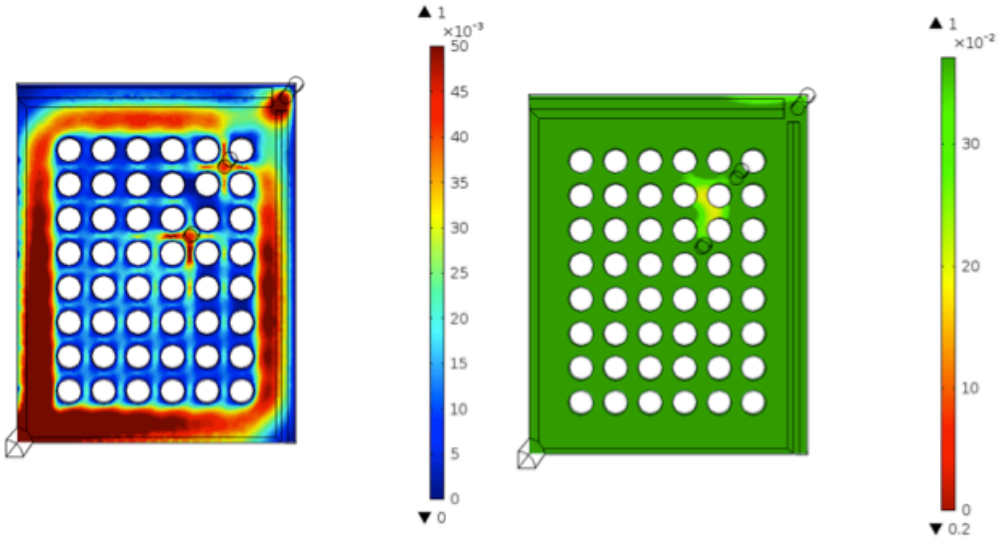

Figure 53 - Velocity and Concentration at Fill FEA Results, 0.635mm Deep Alignment Groove and Additional Groove; u = 0.538 m/s, t_{fill} = 1.7 s

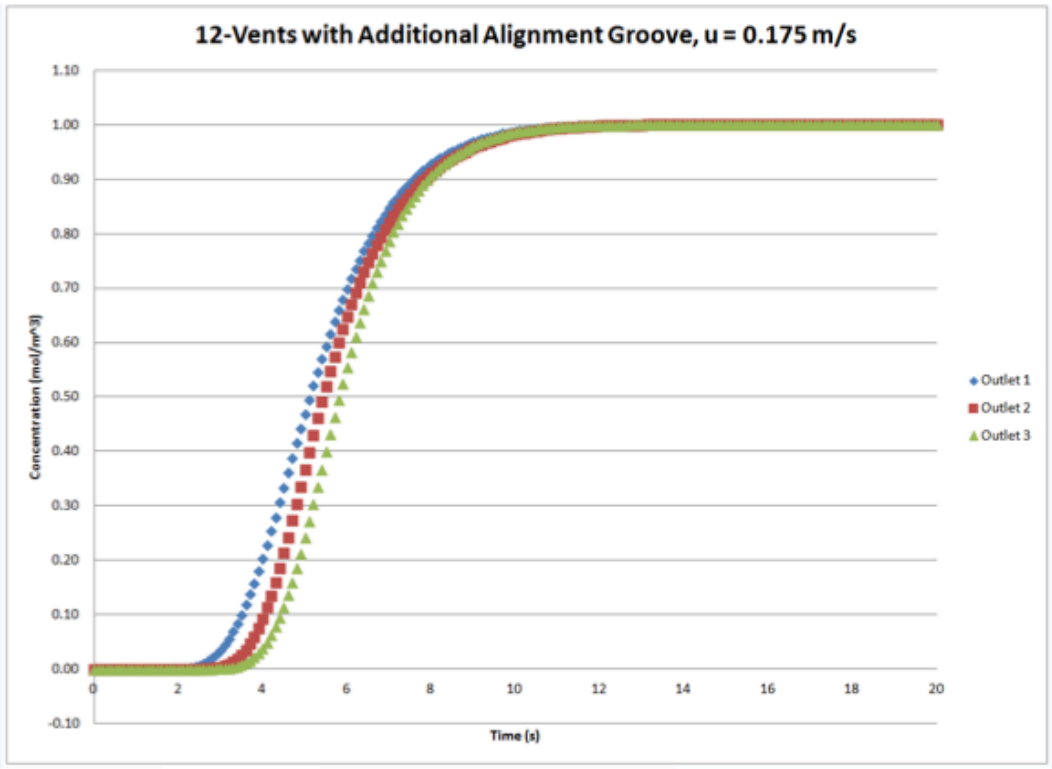

Figure 54 - Concentration vs. Time, 0.635mm Deep Alignment Groove with Additional Groove, u = 0.175 m/s

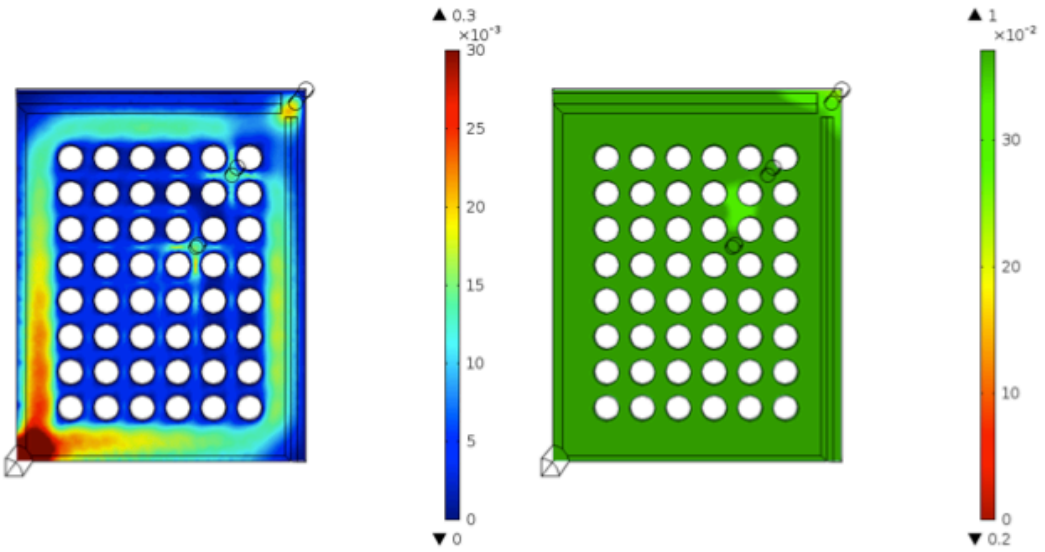

Figure 55 - Velocity and Concentration at Fill FEA Results, 0.635mm Deep Alignment Groove and Additional Groove; u = 0.175 m/s, t_{fill} = 5.0 s

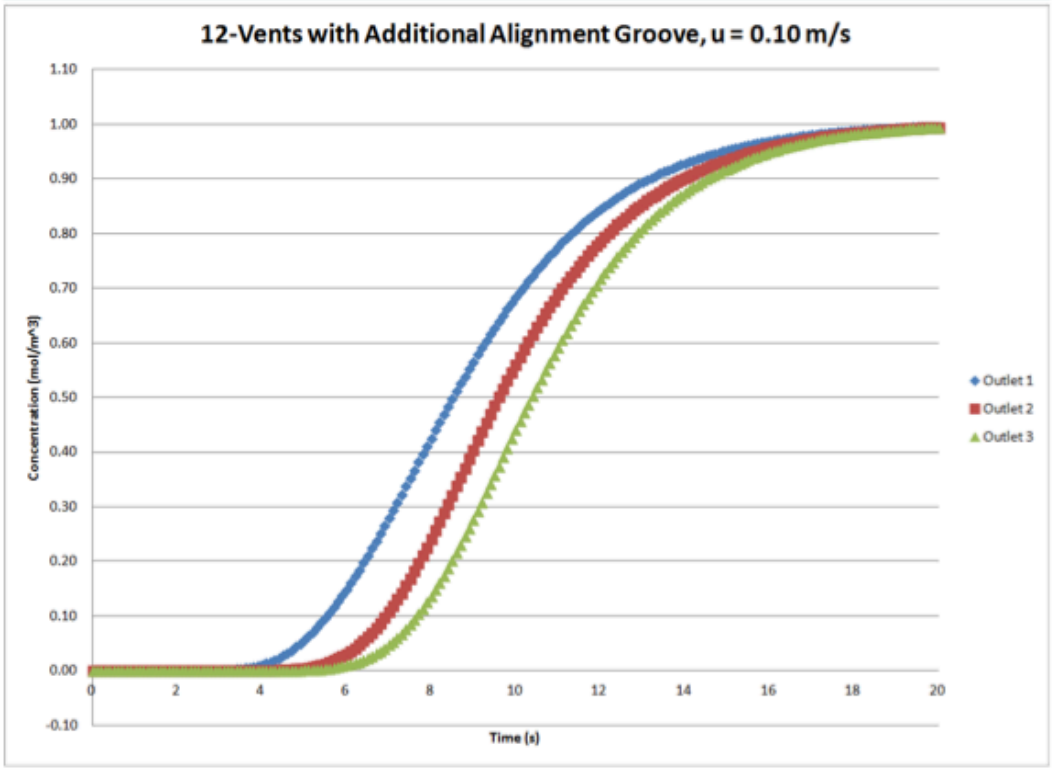

Figure 56 - Concentration vs. Time, 0.635mm Deep Alignment Groove with Additional Groove, u = 0.102 m/s

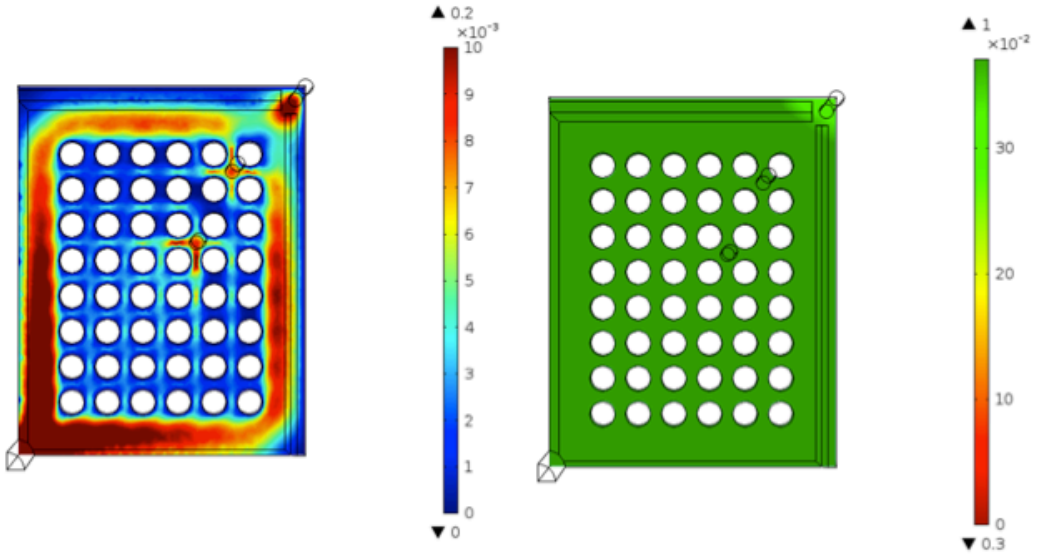

Figure 57 - Velocity and Concentration at Fill FEA Results, 0.635mm Deep Alignment Groove and Additional Groove; u = 0.100 m/s, t_{fill} = 8.9 s

The results in Figure 59 through Figure 66 are for lateral wall geometry. The meshed finite element model for the lateral wall is shown below in Figure 58.

Figure 58 - Finite Element Model, Lateral Wall

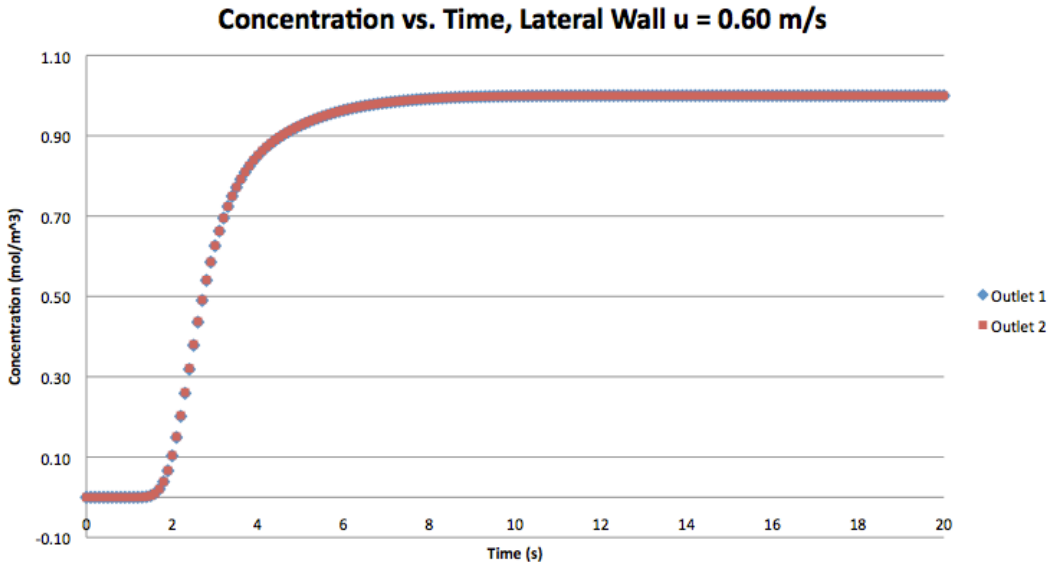

Figure 59 - Concentration vs. Time, Lateral Wall, u = 0.60 m/s

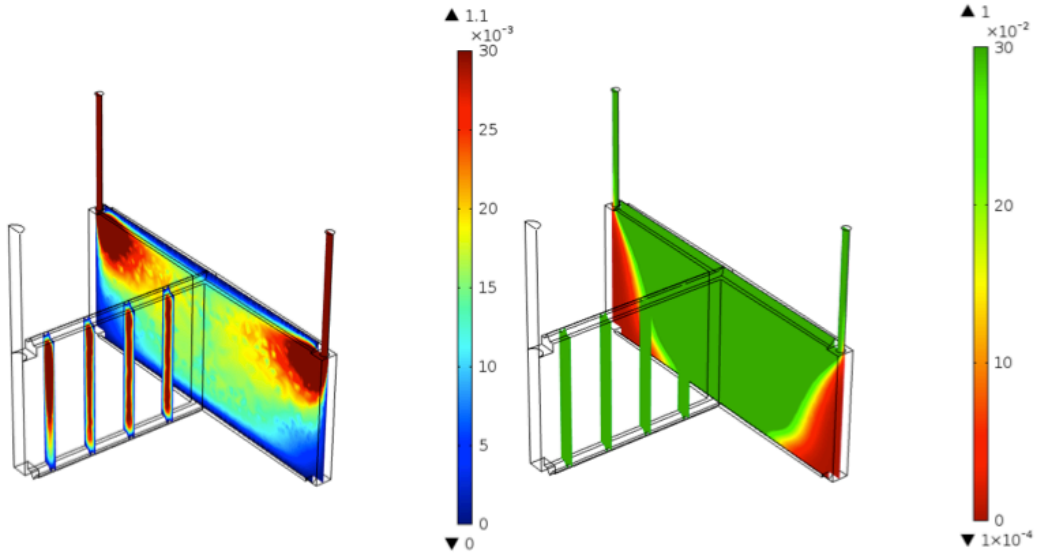

Figure 60 - Steady State Velocity and Concentration at Fill FEA Results; u=0.600 m/s, t_{fill} = 2.4 s

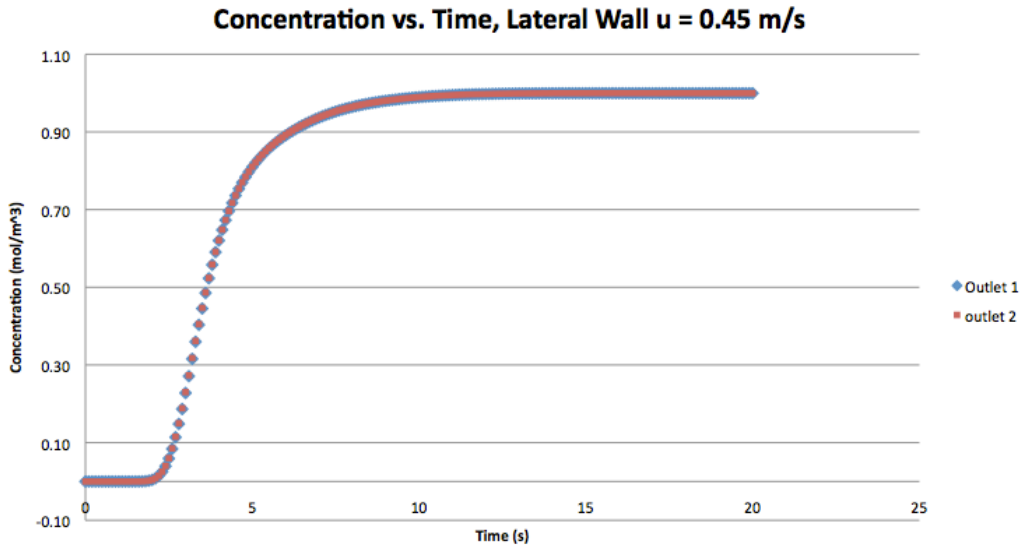

Figure 61 - Concentration vs. Time, Lateral Wall, u = 0.45 m/s

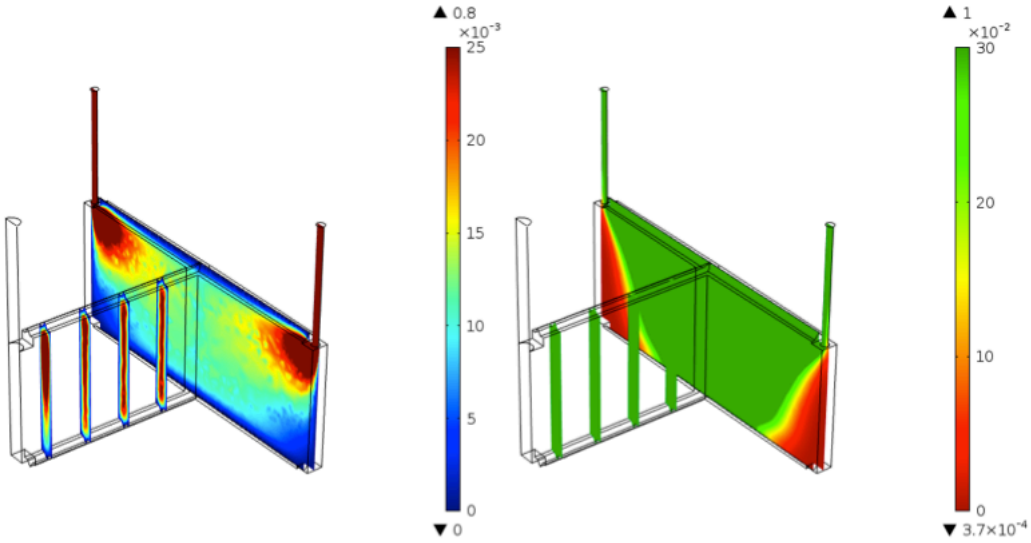

Figure 62 - Steady State Velocity and Concentration at Fill FEA Results; u=0.45 m/s, t_{fill} = 3.2 s

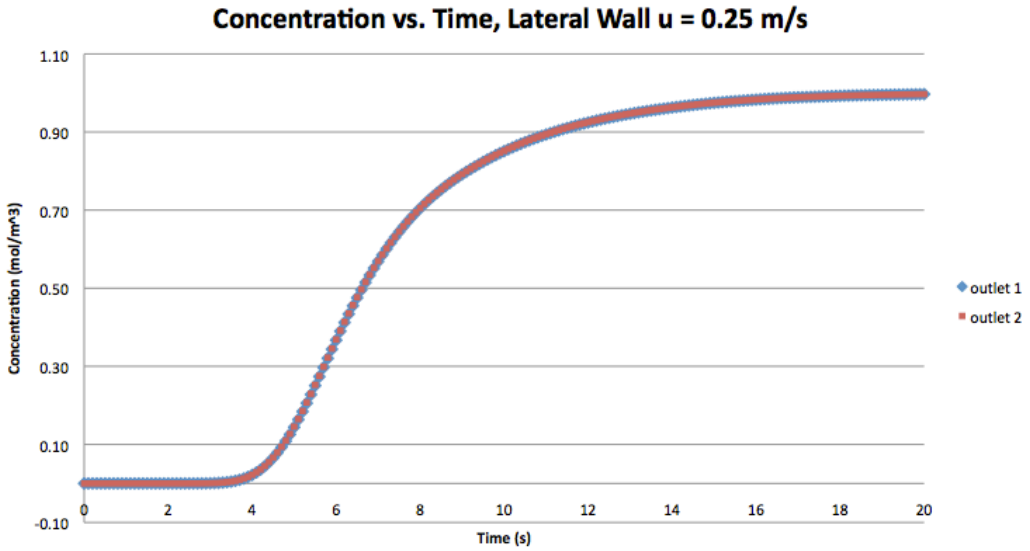

Figure 63 - Concentration vs. Time, Lateral Wall, u = 0.25 m/s

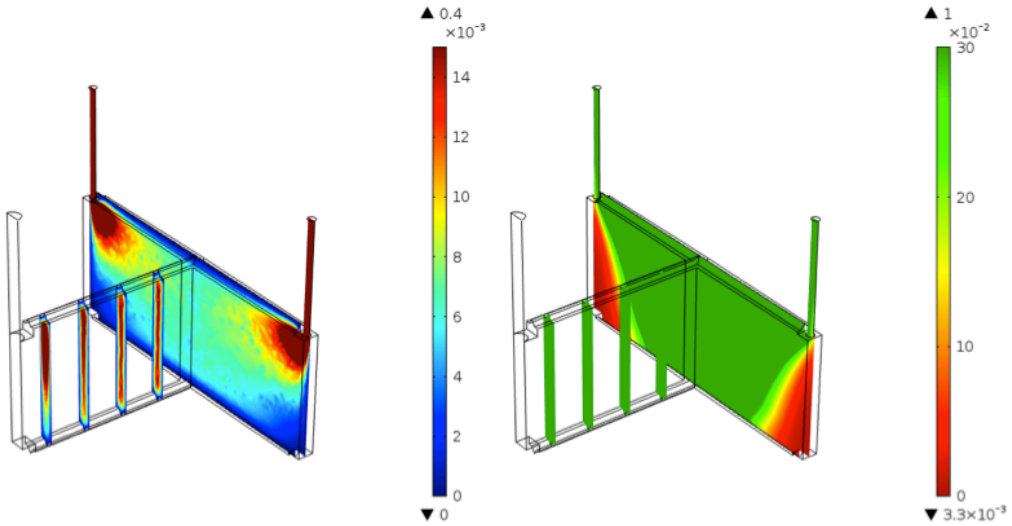

Figure 64 - Steady State Velocity and Concentration at Fill FEA Results; u=0.25m/s, t_{fill} = 5.7 s

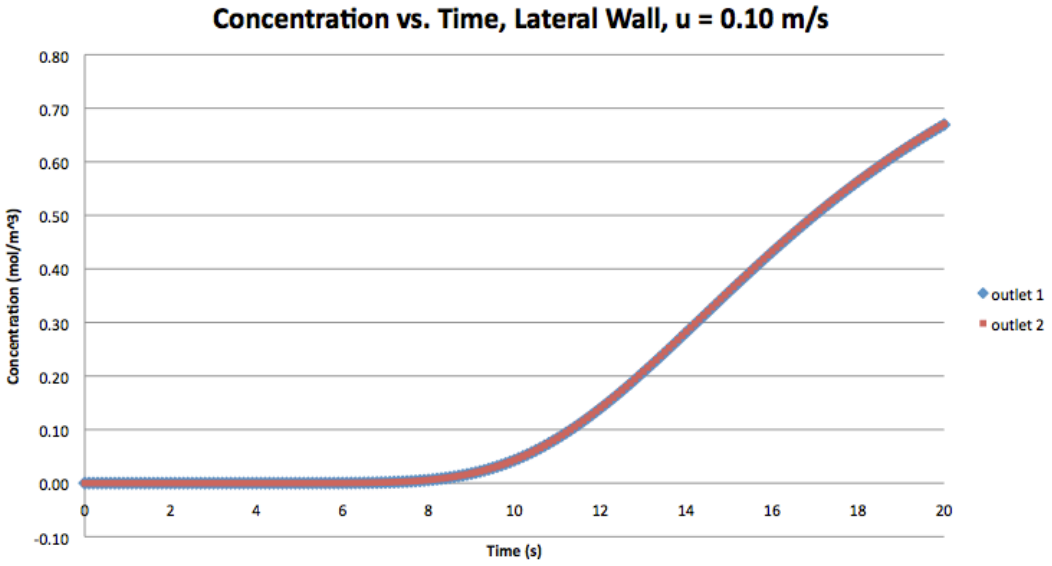

Figure 65 - Concentration vs. Time, Lateral Wall, u = 0.10 m/s

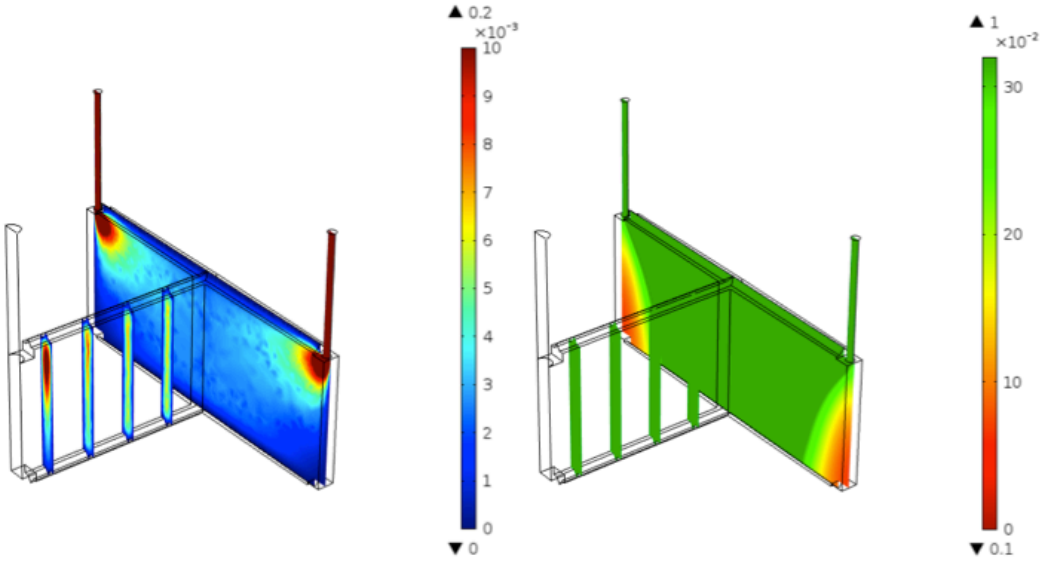

Figure 66 – Steady State Velocity and Concentration at Fill FEA Results; u=0.100 m/s, t_{fill} = 14.9 s

References

[1] Shaffer, Eric. “Translating Translational Research.” *The NIH Catalyst*, July - August 2008.

[2] McGarland, Doris, et al. “Defining Translational Research: Implications for Training.” *Academic Medicine*, March 2010: 470-475.

[3] Charles Ross & Son Co. “Static Mixer Designs and Applications.” *Ross Online.* http://www.staticmixers.com/staticmixer_designs.pdf (accessed Nov. 1 2014).

[4] Heron, M, DL Hoyert, SL Murphy, J Xu, KD Kochanek, and B. Tejada-Vera. “National Vital Statistics Reports.” National Center for Health Statistics, U.S. Department of Health and Human Services, Hyattsville, 2009.

[5] Bolooki, H. Michael, and Arman Askari. "Acute Myocardial Infarction." *Cleveland Clinic.* 12 20, 2014. http://www.clevelandclinicmeded.com/medicalpubs/diseasemanagement/cardiology/acute-myocardial-infarction/.

[6] U.S. Department of Health and Human Services. *About Heart Disease - Consequences & Cost.* http://millionhearts.hhs.gov/abouthds/cost-consequences.html (accessed Dec. 20, 2014).

[7] Carr, ME Jr. “Monitoring of hemostasis in combat trauma patients.” *Military Medicine* 169, no. 12 (Dec. 2004): 11-15.

[8] Mannucci, PM, and M Levi. “Prevention and treatment of major blood loss.” *New England Journal of Medicine*, no. 356 (2007): 2301-2311.

[9] Kolandaivelu, Kumaran, and Deepak L Bhatt. “Antiplatelet Therapy in Coronary Heart Disease Prevention.” *Cardiology Clinics* 29, no. 1 (Feb 2011): 71-85.

[10] Fergusson, DA, et al. “A comparison of aprotinit and lysine analogues in high-risk cardiac surgery.” *New England Journal of Medicine*, no. 358 (2008): 2319-2331.

[11] Martinowitz, U, M Zaarur, BL Yaron, A Blumenfeld, and G Martonovits. “Treating traumatic bleeding in a combat setting: possible role of recombinant activatd factor vii.” *Military Medicine* 169 (12 Suppl), no. 16-8 (Dec 2004): 4.

[12] Goldhaber, Samuel Z., and Nicole Grasso-Correnti. "Treatment of Blood Clots." *Circulation* 106 (2002): e138-e140.

[13] Breet, NJ, et al. “Comparison of platelet function tests in predicting clinical outcome in patients undergoing coronary stent implants.” *Journal of the American Medical Association*, no. 303 (2007): 754-762.

[14] Bhatt, DL. “Intensifying platelet inhibition - navigating between scylla and charybdis.” *New England Journal of Medicine*, no. 357 (2007): 2078-2081.

[15] Dunning, J, et al. “Guidline on antiplatelet and anticoagulation management in cardiac surgery.” *European Journal of Cardio-Thoracic Surgery*, no. 34 (2008): 73-92.

[16] Mohler, ER, 3rd. “Atherothrombosis - Wave goodbye to combined anticoagulation and antiplatelet therapy?” *New England Journal of Medicine*, no. 357 (2007): 293-296.

[17] Bhatt, DL. “Tailoring antiplatelet therapy based on pharmacogenomics: How well do the data fit?” *JAMA*, no. 302 (2009):

896-897.

[18] Gorog, DA, and V. Fuster. “Platelet function tests in clinical cardiology: Unfulfilled expectations.” *J Am Coll Cardiol*, no. 61 (2013): 2115-2129.

[19] Baranek, Sherry L. "The realities of aluminum tooling: using aluminum tooling instead of traditional tools steels reduces cycle time and costs, but requires up-front, open communications between moldmaker, molder, material supplier and hot runner manifold supplier." *MoldMaking Technology* Dec. 2008: 30+. *General OneFile*. Web. 11 Jan. 2015.

[20] Rosato, Dominick, Donald Rosato, and Marlene Rosato. *Injection Molding Handbook.* Norwell, MA: Kluwer Academic Publishers, 2000.

[21] Romeo RIM, Inc. *Reaction Injection Molding Services.* www.romeorim.com (accessed Nov. 8, 2014).

[22] The Society of the Plastics Industry. *Platics Engineering Handbook of the Society of the Plastics Industry.* 5th Edition. Edited by Michael L Berins. Norwell, MA: Kluwer Academic Publishers, 1991.

[23] Kalpakjian, Serope, and Steven R. Schmid. *Manufacturing Processes for Engineering Materials.* Fourth Edition. Upper Saddle River, NJ: Prentice Hall, 2002.

[24] Smooth-On Inc. "Mold Max Series Technical Bulletin." *Smooth-On.* http://www.smooth-on.com/tb/files/Mold_Max_Series_TB.pdf (accessed 12 20, 2014).

[25] Smooth-On Inc. "Smooth-Cast 300 Series Technical Bulletin." *Smooth-On.com.* http://www.smooth-on.com/tb/files/Smooth-Cast_300q,_300,_305___310.pdf (accessed 12 20, 2014).

[26] Rudd, C.D. *Liquid moulding technologies: resin transfer moulding, structural reaction injection moulding, and related processing techniques.* Woodhead Publishing, 1997.

[27] Garcia, MA. *Reactive Mold Filling Modeling.* University of Minnesota, Ann Arbor: UMI Dissertations Publishing, 1991.

[28] Young, WB, RJ Lin, and JL Lee. "Mold filling and cure modeling of RTM and SRIM prcoesses." *Composite Structures*, no. 27 (1994): 109-120.

[29] Castro, JM, CW Macosko, FE Critchfield, EC Steinle, and LP Tacket. "Reaction Injection Molding: Filling of a Rectangular Mold." *Journal of Elastomers and Plastics* 12, no. 1 (Jan. 1980): 3-17.

[30] Blake, John William. *Studies in Reaction Injection Mold Filling (Polymerization) .* University of Minnesota, Ann Arbor: UMI - Dissertations Publishing, 1987.